Optical properties of ultrafine gold particles*

C. G. Granqvist and O. Hunderi†
Physics Department, Chalmers University of Technology, Fack, S-402 20 Gothenburg 5, Sweden
(Received 7 July 1976)

We have prepared spherical and individually isolated gold particles with median diameters in the interval 3 to 4 nm and log-normal size distribution by evaporation in a few Torr of air. The volume fraction of metal was typically 0.3%. Highly reproducible optical transmittance in the range 0.3 to 4 μm was recorded provided the deposits (onto glass substrates) were sufficiently thin to prevent coagulation into large aggregates. A large transmittance minimum was always found at about 0.6 μm, whereas the samples were practically transparent at wavelengths above 1.5 μm. To interpret the measurements we have performed extensive computer calculations based on the effective-medium theories by Maxwell-Garnett (as extended by Polder and van Santen), Bruggeman, and by Hunderi. These theories are indistinguishable in the limit of small filling factors. As input data we have used bulk results, for which the Drude part was modified to account for a size-limited electron mean free path assuming diffuse boundary scattering. The calculated wavelength-dependent transmittances displayed a minimum whose distinctness was strongly dependent on the median particle diameter, whereas the distribution width or shape played a subordinate role. The computed results could be brought into fair agreement with the experiments provided we invoked an apparent plasma frequency for the particles which was lower than the bulk value and an effective sample thickness of the order of twice the measured one. To explain the meaning of this seemingly *ad hoc* procedure we have calculated (using unshifted plasma frequencies and sample thicknesses) the effects of a dielectric coating on the particles and of deviations from nonspherical shapes. Neither can be reconciled with all the experimental evidence. We finally considered the role of dipole-dipole coupling which is significant despite the small filling factors because the gas evaporated particles must be touching. This interaction is accounted for approximately by a set of effective depolarization factors pertaining to each of a number of well-defined geometrical configurations of spheres. Assuming the deposits to consist of a mixture of close-packed clusters, infinite linear chains, and independent single particles (i.e., by use of two adjustable parameters solely, whose magnitudes were supported by electron micrographs), we were able to reproduce the experimental transmittance data to within a few percent over the entire wavelength interval. The remaining deviations were presumably caused by our simplified treatment of the dipole-dipole interaction, and hence there appears to be no effects due to size quantizations.

I. INTRODUCTION

This paper reports on an extensive experimental and theoretical study of the optical properties of ultrafine gold aggregates produced by gas evaporation. The wavelength range 0.3 to 4 μm was investigated for spherical particles with mean diameters of 3 to 4 nm.

As a convenient introduction Fig. 1 serves to illustrate the drastically differing optical properties which can be achieved by preparing Au deposits under different experimental conditions. The solid curve, which is of primary interest in connection with the present work, originates from a layer of ultrafine and individually isolated gold particles prepared by evaporation in the presence of air, such that a dielectric coating was obtained on their surfaces. The most noteworthy features are the transmittance minimum (sometimes referred to as the "anomalous absorption band") at a wavelength of about 0.6 μm, and the fact that the deposit is virtually transparent (absorptance $<3\%$) at $\lambda > 1.5$ μm. A principally different behavior is encountered for Au particles grown by vaporization in a pure noble gas where touching particles are electrically connected; as seen from the dashed curve in Fig. 1 the transmittance exhibits only a very weak dependence on λ. For comparison we have also plotted measured data for a continuous gold film (dotted curve) which hence represents bulk properties; by going to smaller wavelengths the transmittance is first enhanced, as predicted from free-electron (Drude) theory, but beyond $\lambda = 0.51$ μm a sharp decrease occurs owing to the onset of interband transitions.

The main purpose of this paper is *to develop the experimental and theoretical analyses for the deposits consisting of isolated particles* to an extent such that the measured transmittance curves agree quantitatively with calculated data over the entire wavelength interval. This accurate agreement has implications not only for gas evaporated particles, but the occurrence of anomalous absorption is a very general phenomenon, which has been observed frequently for noble-metal grains. In the previous investigations the particles were prepared by several different tech-

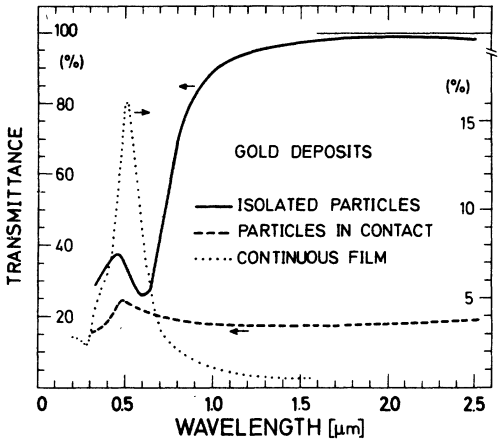

FIG. 1. Comparison of measured transmittance vs wavelength for perpendicular incidence onto gold deposits. Films were produced by evaporation in 2 Torr of air to make individually isolated particles (sample No. 20 *B*; the preparation will be discussed in Sec. II A), by evaporation in 2 Torr of pure N_2 to get particles in electrical contact (sample No. 21 *A*) or by preparing a 48-nm-thick continuous film under good vacuum conditions. Note the different vertical scales for the curves (as indicated by arrows).

niques: (a) by making colloids suspended in an aqueous solution,[1-3] a glass matrix,[3-9] KCl,[10,11] gelatin,[12] polymethylacrylate,[13] or butanol[14]; (b) by island growth in discontinuous films[15-25]; (c) by preparing granular cermet films[26-28] comprised of noble metal and SiO_2; and, for a few works, (d) by gas evaporation in the presence of oxygen.[29-33]

We have chosen the latter technique as this appears to be the only one for which highly reliable sizes and size distributions can be obtained for single crystalline particles, and where complicating effects from the medium surrounding the particles can be avoided.

The layout of this article is as follows: In Sec. II we describe the experimental details regarding particle production and characterization by optical- and transmission-electron microscopy. The discussion is fairly detailed as motivated by the importance to get accurate sizes as well as appropriate dielectric coatings on the particles (cf. the solid and dashed curves in Fig. 1). The occurrence of aggregation effects, i.e., the formation of chains and clusters, is pointed out. Optical transmittance measurements are reported in Sec. III; the good reproducibility of the data is stressed. The foundations for our theoretical description is outlined in Sec. IV where we treat effective-medium theories. A general criterion for their validity is followed by a discussion and comparison of the different formulations. A series of calculations based on these effective medium theories and bulk data for gold (modified to account for a small mean free path of the electrons) is presented in Sec. V. It is found that the theoretical and experimental results can be brought into fair agreement provided we (i) use a fictitious plasma frequency for the particles which is lower than in the bulk and (ii) invoke an effective optical thickness for the sample which has about twice the measured value. The physical background of (i) and (ii) is treated in Sec. VI where we consider the roles of oxide coating, nonspherical shapes, and dipole-dipole coupling among neighboring particles. Only the latter effect is found to be significant. Postulating that a given particle acts as a member of a close-packed cluster or an infinite chain or behaves as an independent entity for the dipole-dipole interaction (i.e., by use of two free parameters) we are able to fit the theoretical and experimental results to within a few percent over the whole wavelength range. We are thus able to properly account for the observed transmittance data without incorporating any size quantization effects. The main conclusions are summarized in Sec. VII where we also give some final remarks. Some preliminary results of the present work were reported previously in Ref. 34.

II. SAMPLE PREPARATION AND MICROSCOPY

A brief description of the evaporation technique (Sec. A) is followed by a discussion of sample characterization using optical microscopy (Sec. B) as well as high resolution electron microscopy (Sec. C). The occurrence of log-normal size distributions is pointed out in Sec. D.

A. Evaporation

The ultrafine particles were prepared by evaporation of gold (purity 99.99%) from a tungsten boat in a conventional bell-jar system. The vacuum chamber was first evacuated to approximately 10^{-5} Torr by use of an oil diffusion pump. After closing the pumping valve air was introduced to the pressures listed in Table I for the various samples. The metal atoms, which are effused from the heated vapor source, lose their energy rapidly by collisions with the gas atoms, such that a highly supersaturated state is reached from which stable clusters of metal atoms are produced by homogeneous nucleation. These embryonic particles then grow by liquid-like coalescence to form larger grains whose ultimate size is governed by several experimental conditions like evaporation rate, atomic (or molecular) weight for the gas, its pressure, etc. The coales-

TABLE I. Data for the Au particle samples. These were prepared by evaporation at a pressure p of air to give deposits having a weight per unit area W/A and a filling factor f. The log-normal size distributions were characterized by a median diameter $\bar{x}$ and a dimensionless geometric standard deviation σ.

Sample	p (Torr)	W/A (g/m^2)	f (%)	$\bar{x}$ [nm]	σ
18 *G*	2	0.29	0.32±0.05	3.5	1.37
18 *H*	2	1.36	•••	•••	•••
19 *A*	2	0.32	0.37±0.06	3.4	1.35
19 *B*	2	0.80	0.28±0.06	•••	•••
19 *D*	2	0.91	0.43±0.06	•••	•••
20 *A*	2	0.36	0.27±0.05	4.0	1.34
20 *B*	2	0.55	0.49±0.08	3.3	1.40
20 *C*	6	•••	•••	4.0	1.36
20 *E*	6	0.77	•••	3.9	1.38
21 *A*	2[a]	•••	•••	•••	•••
26 *A*	6	•••	•••	•••	•••

[a] Evaporated in pure N_2.

cence process is supposed to be very rapid owing to melting point depression[35] in small particles and heating caused by radiation from the vapor source. A detailed discussion of the gas evaporation technique can be found in Refs. 36–38.

In our experimental setup the particles were collected on a glass substrate (microscope slide 76×26×1 mm^3) positioned 8 cm above the vapor source. A shutter covered the substrate while the tungsten boat was heated; it was withdrawn when the evaporation was going under steady conditions and kept open until the coating on the glass surface showed a suitable decrease of transmission as judged from visual inspection. In practice this time was $\frac{1}{4}$ to 1 min. The shutter was then brought back to its initial position and the heating was turned down. The bluish particle deposits on their glass backings were now ready for optical transmission studies. The W boats were attacked by the air and each lasted usually only for two or three evaporations.

A simple resistance measurement for particle films obtained by evaporation in air did not give any measurable reading. It was estimated that the resistivity was $\gg 10^4$ Ωm, from which it is clear that no continuous metallic path was formed along the whole film. If particles were prepared by evaporation in pure nitrogen, the resistivity was several orders of magnitude lower; hence the particles were then connected. These findings are supported by similar results of Harris[30,31] and McKenzie.[33]

B. Optical microscopy

The gold deposits were investigated by optical microscopy using a Leitz "Orthoplan" universal large-field microscope operated in transmitted light. A set of pictures taken in the microscope is reproduced in Fig. 2. Part (a) was obtained by focusing in the substrate plane. It is seen that the coverage is not even but rather seems to be of a flocculant nature with typical distances between the clusters of the order of 10 μm. The lighter regions indicate a decrease in the density but not a total absence of particles; indeed, pinholes were seen only occasionally and were always caused by contamination on the substrates. Part (b) was taken by focusing 3.5 μm above the substrate plane and (c) by increasing this distance to 7 μm. When focusing 10.5 μm above the glass surface only a blurred image could be seen. The set of pictures proves that the deposits resemble a hilly landscape with summits up to a height of approximately 10 μm. Schematic cross sections of such a structure are depicted in the upper part of Fig. 2 where we also indicate the location of the focal planes. It is interesting to note the principal similarity with the Stranski–Krastanov growth model which has been suggested[39] for the buildup of a discontinuous or semicontinuous film.

The small depth of field for the optical microscope made it possible to determine the thickness t of the particle films as is evident from Fig. 2. These data were combined with measurements of deposited mass per unit area W/A, obtained by weighing the sample before and after wiping off the Au deposit from part of the substrates; results are given in Table I. From these two quantities the filling factor f, i.e., the fraction of the sample volume occupied by particles, is given by

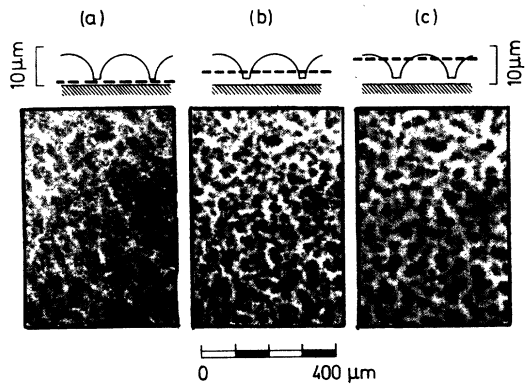

FIG. 2. Microscope images of the same region of a gold deposit prepared by evaporation in air (sample No. 20 *B*). Schematic upper pictures show a cross-sectional view of particle layers on glass substrates. Dashed lines indicate focal planes for the microscope.

$$f = (W/A)(\rho t)^{-1}, \quad (1)$$

where ρ is the density of bulk gold. Values for f are included in Table I. It is important to note that, whereas t and f can be determined independently only to ±25%, say, *the product ft is accurately known* as it is given only by W/A which has a more precisely measured value. This observation is important as will become clear from the discussion of optical transmittance later in the paper.

Our determination of f proves that only about $\frac{1}{300}$ of the sample volume consists of gold particles. Filling factors of the same order of magnitude have been reported also by others.[29-32] For deposits which were scraped off their substrates considerably larger f's have been noted,[40] which is probably caused by a partial collapse of the structure for freely supported particles as discussed in the Appendix.

C. Transmission electron microscopy

An electron-microscope grid covered with a carbon film was placed in the immediate vicinity of the substrate and was exposed to the particles simultaneously with the glass surface. Hence very reliable samplings of the actual particle sizes were possible. Figure 3(a) shows a typical bright field picture taken at a magnification of 130 000× with a Philips EM 300 electron microscope operated at 100 kV. The particles are well rounded and very small (mean diameters of about 3 nm). They exhibit a size distribution. The individual particles are connected into chains and clusters; this is a characteristic feature of gas-evaporated particles[36-38] which may be caused by van der Waals interaction as well as by electrostatic attraction. By viewing the particles in dark-field mode, it was shown that they were single crystalline with no traces of stacking faults or other imperfections.

Figure 3(b) reproduces an electron diffraction image taken in the microscope. Owing to the very small particle sizes no spots were visible but only broadened Debye rings signifying that the main constituent of the sample was fcc Au. In addition there was one diffuse ring close to the central spot which we ascribe to WO_3. It became increasingly manifest when the evaporations were performed at enhanced air pressures, and for vaporization at $p > 10$ Torr a yellowish taint on the particle coatings—indicative of yellow tungsten trioxide—was sometimes visible. Evidently this contamination by volatile WO_3 stems from the evaporation source.

The presence of some tungsten oxide in gas evaporated Au particles has been noted[30-33,41,42] before, and recently McKenzie[33] has claimed that this oxide is the reason for the high resistivity of the samples. We carried out dark-field electron microscopy which proved that the diffraction line indicating WO_3 resulted from particles of about the same size as for Au interdispersed among these, whereas no trace of any coating on the gold grains could be documented. This ob-

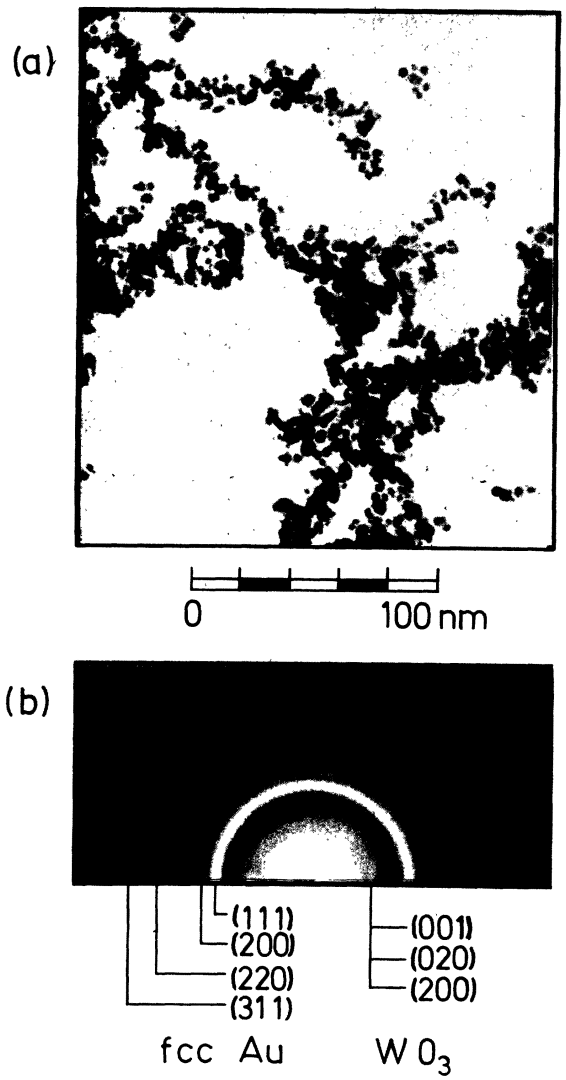

FIG. 3. Part (a) depicts ultrafine gold particles prepared by evaporation in air (sample No. 20 *B*). Note the clusters and chains! Grainy background is caused by structure in the supporting carbon layer. Part (b) shows electron diffraction from the same sample. Calculated positions for the four innermost reflections of fcc Au are indicated; these agree with the measured radii. Correspondence was obtained also for the line intensities. Weak line closest to the center is due to three overlapping reflections from triclinic and/or orthorhombic WO_3 (cf. Ref. 44).

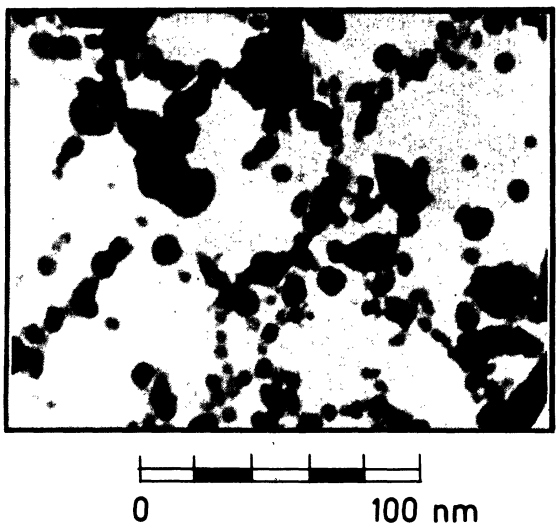

FIG. 4. Coagulated gold particles prepared by evaporation in air (sample No. 18 *H*). Largest particles exhibit a tendency towards hexagonal images which is probably indicative of their being three-dimensional icosahedrons (cf. Ref. 45).

servation is interesting as our optical transmittance data (to be reported on in Sec. III) can be fitted to theory only if an insulation of the *individual* particles is postulated. A monolayer of WO_3 on the surfaces cannot be ruled out *a posteriori*, but we feel that a more plausible hypothesis is that an extremely thin coating of gold oxide,[43] which might be formed during the growth in air, provides the isolation on a microscopic scale. In a effort to avoid the complication of tungsten trioxide we tried to vaporize gold also from molybdenum and tantalum boats. These attempts were unsuccessful, though, as the sources invariably were burnt off before any significant evaporation took place.

The particle films were very sensitive to heating and for thick deposits (in practice $W/A \gtrsim 0.7$ g/m^2) it appeared that radiation from the vapor source was sufficient to promote coagulation into larger aggregates. An extreme case is shown in Fig. 4 which depicts gold particles for the thickest of our samples on the same magnification as in Fig. 3(a). The coagulation also affected the optical properties drastically as will be discussed below.

D. Size distributions

We evaluated particle sizes for the samples consisting of noncoagulated granules from high-resolution electron micrographs similar to Fig. 3(a). A typical size distribution is indicated by the circles in Fig. 5, from which it is clear that the diameters x have a skew bell-shaped distribution with a tail towards the large diameter side.

Size distributions for gas evaporated particles have been investigated recently,[38,46] and it was shown that the fractional number of particles Δn per logarithmic diameter interval $\Delta(\ln x)$ could be approximated accurately by

$$\Delta n = \frac{1}{(2\pi)^{1/2} \ln\sigma} \exp\left[-\frac{1}{2}\left(\frac{\ln(x/\bar{x})}{\ln\sigma}\right)^2\right]\Delta(\ln x), \qquad (2)$$

i.e., by a log-normal distribution function characterized by a median diameter $\bar{x}$ and a geometric standard deviation σ. This particular distribution has been derived[38,47] for particles growing by binary collisions accompanied by liquid-like coalescence using general statistical concepts. The log-normal distribution has been applied successfully also to island structures in discontinuous noble metal films[38,47,48] and to particles in supported metal catalysts.[49]

The good correspondence between experimental data and the log-normal distribution is proved for the present samples by Fig. 5. Results of $\bar{x}$ and σ for similar fits, performed on the other samples, are given in the two last columns in Table I. Our evaporation conditions resulted in particles with

$$3.3 \leq \bar{x} \leq 4.0 \text{ nm}$$

and

$$1.34 \leq \sigma \leq 1.40.$$

This interval for σ compares rather well with

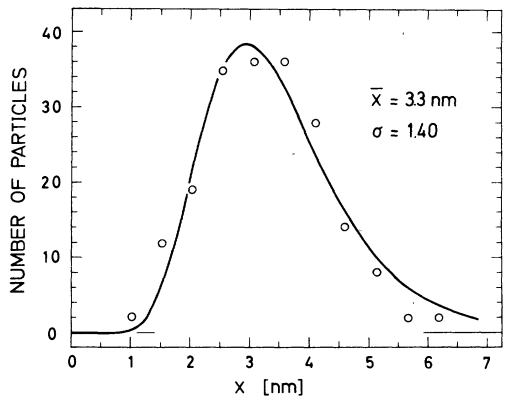

FIG. 5. Diameter distribution for gold particles prepared by evaporation in air (sample No. 20 *B*). Circles denote staple midpoints in a size histogram based on an evaluation of about 200 particles. Bell-shaped curve represents a fit to a log-normal distribution characterized by the shown values of $\bar{x}$ and σ. Area under the log-normal graph is put equal to the area under the histogram curve.

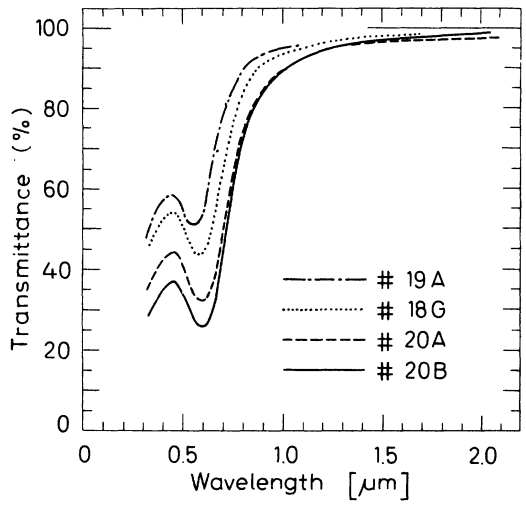

FIG. 6. Measured wavelength-dependent transmittances for four gold deposits prepared by evaporation in air. Sample No. 20 *B* was reported on earlier in Figs. 3(a) and 5.

a previous extensive investigation[38] of size distributions for gas evaporated particles of many different metals which invariably gave σ's between 1.36 and 1.60.

III. TRANSMITTANCE MEASUREMENTS

Optical transmittance in the wavelength intervals $0.33 < \lambda < 2.5$ μm and (in some cases) $2.5 < \lambda < 4$ μm was measured with a UNICAM SP 700, respectively, a BECKMAN IR 10, double-beam spectrophotometer. These wavelength ranges were dictated by the transmittance of the glass substrates. In order to significantly decrease the influence from the glass, we always put a substrate with particle coating in one of the light beams and a clean substrate in the other and monitored the ratio between the two transmitted intensities.

Figure 6 shows wavelength-dependent transmittances for four samples with different values of W/A. None of these samples exhibited any coagulation effects but their electron micrographs were all similar to Fig. 3(a). The most noteworthy feature is the dip in the transmittance at a wavelength λ_{min} in the range

$$0.56 < \lambda_{min} < 0.60\ \mu\text{m}.$$

The corresponding transmittances T_{min} vary between 26% and 52% for these particle films. We also note that *the overall reproducibility of the curves is excellent*. This observation if of utmost importance as the rest of the paper is devoted to the detailed theoretical description of this kind of data.

In Fig. 7 we plot the magnitude of T_{min} as a function of W/A. The good fit of our data points to a straight line shows that a relation

$$T_{min} = e^{-\gamma W/A} \tag{3}$$

is obeyed. The constant γ has the numerical value

$$\gamma = 2.5\ \text{m}^2/\text{g}.$$

Hence all the samples can be described by a unique attenuation constant, which by Eq. (1) is equal to $\gamma f \rho$. This shows again the good reproducibility. In Fig. 7 we have also plotted T_{min}'s extracted from the literature.[29–33] All these data are in fair correspondence with ours. A linear extrapolation for Harris's[29,30] results indicates that $\gamma \approx 3$ m^2/g for his samples.

The high reproducibility of the optical data, which was proved for noncoagulated particles by Fig. 6, is no longer found for gold deposits prepared under conditions such that large particles are formed (for example, by heating). This result is elucidated in Fig. 8 where the transmittance data range from curves with strong similarities with the previous ones, as for No. 20 *C* where only a small fraction of coagulated grains was present in the sample, to very smeared plots when essentially all the particles had coalesced into large aggregates, as for No. 18 *H* for which an electron micrograph was reproduced in Fig. 4. With these results as a background it

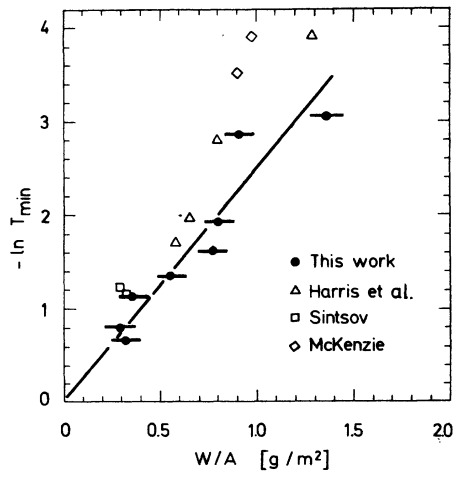

FIG. 7. $-\ln T_{min}$ vs W/A for gold deposits prepared by evaporation in air. Filled circles for the four lowest W/A's refer to the same samples as in Fig. 6. Horizontal bars indicate estimated uncertainties in the determination of weight per unit area. Straight line represents Eq. (3). In addition to our data we have plotted results by Harris *et al.* (Refs. 29–31), Sintsov (Ref. 32), and McKenzie (Ref. 33).

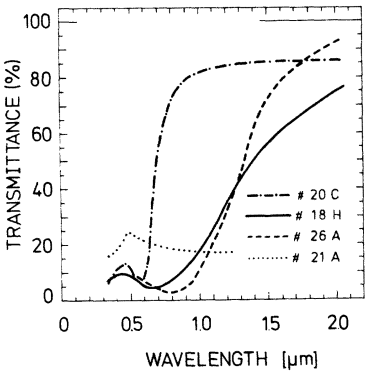

FIG. 8. Wavelength-dependent transmittances for gold deposits prepared by evaporation in air (samples Nos. 20 *C*, 18 *H*, and 26 *A*) and in pure nitrogen (sample No. 21 *A*; cf. also Fig. 1). Three former deposits consisted of coagulated particles.

is interesting to turn to the literature where transmittance curves with at least qualitative similarities with our Figs. 6 and 8 have been plotted in articles by Harris *et al.*,[29] Harris and Beasley,[30] Sintsov,[32] and McKenzie.[33] Quite generally their graphs exhibit wider transmittance dips than for the deposits of our Fig. 6, and furthermore this smearing appears to get progressively larger as the *W/A*'s are increased. Judging from the published[29,30,33] electron micrographs the particles appeared rather coagulated (presumably caused by excessive heating) in which case their optical data can be reconciled with ours.

A qualitatively different behavior, compared with all previous samples of this section, was observed for deposits prepared in a pure inert gas, where no dielectric coating on the particles was obtained. For such deposits a small peak in the transmittance was seen at $\lambda \approx 0.5$ μm, whereas the rest of the investigated wavelength interval displayed an almost constant transmittance; cf. sample No. 21 *A* in Fig. 8. Generally speaking this type of deposit (usually referred to as "gold blacks" in the literature), has been studied more extensively than the ones made by evaporation in the presence of oxygen. As reported in numerous works[29-33,41,42,50-52] the constant transmittances extend up to λ's of at least 40 μm, i.e., deeply into the infrared regime. The previous interest was caused by the very efficient heat absorption properties which were first exploited for use in high-speed bolometers.[53-55] Here we contend ourselves with noting the very different behavior compared with the previous deposits; the "gold blacks" will not be treated further in this paper.

IV. EFFECTIVE MEDIUM THEORIES

For the gas evaporated gold samples the diameters of the individual particles are always orders of magnitude smaller than any wavelengths of the relevant electromagnetic radiation. This shows that the optical properties of the deposits may be described in terms of an *effective medium*. In this section we first derive a criterion for the general applicability of the effective medium approach (Sec. A), which appears to have escaped mentioning before. We then discuss different theoretical models[56] for the effective medium (Sec. B) and treat the formulations by Maxwell-Garnett,[57] Bruggeman,[58] and Hunderi,[59] including subsequent developments of the former two. The theories are compared in Sec. C; in the limit of small filling factor they are found to give indistinguishable results.

A. Validity of the effective medium approach

In order for the effective medium concept to be of general applicability we require that it should be *unique*, i.e., it should *not* be a function of the particular experimental conditions. To estimate an upper limit of the particle diameter for which *transmittance* and *reflectance* data can be accounted for by an effective medium characterized by the same parameters, we calculate the scattered fields from the particles by use of Mie's theory,[60] which is an exact solution of Maxwell's equations for scattering of a plane wave by a homogeneous sphere of arbitrary size. This field can then be inverted to yield an apparent dielectric permeability for the effective medium by the same approach as taken previously[59] by one of the authors in a calculation of the influence from grain boundaries on the reflectivity of a metal surface.

We consider a thick slab of material which contains independently scattering particles. An incident plane wave with a field amplitude U_0 gives rise to a back-scattered field amplitude[61]

$$i\pi U_0 \rho_p S(\pi)/k^3,$$

where $k \equiv 2\pi/\lambda$ is the wave vector, $S(\theta)$ is the amplitude function for a scattering angle θ, and ρ_p is the number of particles per unit volume which is taken to be small. This field corresponds to a formal refractive index $\bar{N}_R$ for the medium being[59]

$$\bar{N}_R = \frac{1 - i\pi\rho_p S(\pi)/k^3}{1 + i\pi\rho_p S(\pi)/k^3} \doteq 1 - i2\pi\rho_p S(\pi)/k^3. \qquad (4)$$

A transmission measurement on the same slab would yield[61]

$$\bar{N}_T \doteq 1 - i2\pi\rho_p S(0)/k^3. \quad (5)$$

Hence if $S(0)$ differs appreciably from $S(\pi)$, no unique refractive index is obtained and, by the above criterion, there exists no meaningful effective medium. The ratio $S(\pi)/S(0)$ has been evaluated from Mie's theory by van de Hulst,[61] who found the result

$$\frac{S(\pi)}{S(0)} = 1 + \frac{k^2x^2}{15}\,\frac{(\epsilon+4)(\epsilon+2)}{2\epsilon+3} + O(k^4x^4), \quad (6)$$

where ϵ is the dielectric permeability of the particles.

If both the real and imaginary parts of the second term in Eq. (6) shall be smaller than 5%, say, the particle radius must be less than about 10 nm for typical values of ϵ and k; this is generously fulfilled for our samples (cf. Table I). The requirement is equivalent to neglecting higher-order multipole effects.

B. Theories

The simplest approach to the description of the dielectric properties of a multiphase mixture was given by Maxwell–Garnett[57] (MG), who used the theory originally designed by Clausius and by Mosotti to account for color changes in discontinuous noble-metal films. The effective dielectric permeability $\bar{\epsilon}^{MG}$ is given by

$$\frac{\bar{\epsilon}^{MG} - \epsilon_m}{\bar{\epsilon}^{MG} + 2\epsilon_m} = f\,\frac{\epsilon - \epsilon_m}{\epsilon + 2\epsilon_m}, \quad (7)$$

for spherical particles dispersed in a surrounding medium characterized by a dielectric constant ϵ_m. Equation (7) was derived under the assumptions that the separation of the particles is sufficiently large to ensure independent scattering and that the Lorentz local-field correction applies. A straightforward extension to ellipsoidal particles has been published in several papers.[27,62,63] Principally owing to its simplicity the MG theory has been used frequently in treatments of optical properties of fine noble-metal particles[3,5,14,19,22,24,27,28,64]

In a dielectric mixture only part of the internal field is effective in directing the dipoles as shown by Onsager.[65] His "reaction field" theory was used by Böttcher[66] to derive an improved effective medium permeability for spherical particles, and the generalization to ellipsoidal shapes was given by Polder and van Santen[67] (PvS). The calculations by the latter authors may be combined with the MG approach to yield an effective permeability $\bar{\epsilon}^{MG\text{-}PvS}$ by the relation

$$\bar{\epsilon}^{MG\text{-}PvS} = \epsilon_m\,\frac{1 + \frac{2}{3}\sum_j f_j\alpha_j}{1 - \frac{1}{3}\sum_j f_j\alpha_j}. \quad (8)$$

The subscript j denotes particles belonging to the jth column in a size histogram centered at a diameter x_j and the f_j's are a set of fractional filling factors normalized by $\sum_j f_j = f$. α_j is proportional to the polarizability of particles in the jth class and for an ellipsoidal shape it is given by[68]

$$\alpha_j = \frac{1}{3}\sum_{i=1}^{3}\frac{\epsilon_j - \bar{\epsilon}}{\bar{\epsilon} + L_i(\epsilon_j - \bar{\epsilon})}, \quad (9)$$

where the L_i's are the depolarization factors for the jth particles ($\bar{\epsilon}$ with no superscript denotes any of the effective medium permeabilities of this section). To first order the self-consistent Eq. (8) reduces to Eq. (7) for identical spheres, i.e., when $L_1 = L_2 = L_3 = \frac{1}{3}$. It is important to note that, though an improvement over the simple MG approach, the MG-PvS theory should be restricted to small filling factors.

Another self-consistent effective medium theory, which in principle should be valid for all f's as it treats the components in the mixture on an equal basis, was originally put forward by Bruggeman[58] and has since been rediscovered by Odelevskii[69] and by Landauer.[70] In recent years the theory has been discussed by Kirkpatrick,[71] Elliott *et al.*,[72] and, in particular, by Stroud.[73] The Bruggeman theory has been successful in explaining[70,74] experimental data on resistivity and low-field Hall coefficient of inhomogeneous media but, to our knowledge, no application to optical properties has yet been published. The basic condition of the Bruggeman (BR) theory is that the first-order scattering shall vanish on the average, i.e., the self-consistent local field is equivalent to the choice of an active medium such that the average single-site scattering is zero. This points up a close analogy with the well-known coherent-potential approximation for alloys. The effective medium permeability $\bar{\epsilon}^{BR}$ is given by

$$\bar{\epsilon}^{BR} = \epsilon_m\,\frac{1 - f + \frac{1}{3}\sum_j f_j\alpha_j}{1 - f - \frac{2}{3}\sum_j f_j\alpha_j}, \quad (10)$$

which has apparent formal similarities with the corresponding equation for the MG-PvS theory, i.e., Eq. (8). For a two-component mixture characterized by ϵ and ϵ_m, Eq. (10) reduces to

$$f\,\frac{\epsilon - \bar{\epsilon}^{BR}}{\epsilon + 2\bar{\epsilon}^{BR}} + (1-f)\,\frac{\epsilon_m - \bar{\epsilon}^{BR}}{\epsilon_m + 2\bar{\epsilon}^{BR}} = 0, \quad (11)$$

which is a simple second-order equation for $\bar{\epsilon}^{BR}$.

Finally, the apparent dielectric function from the back-scattered fields, as shown recently by Hunderi,[59] yields still another expression for the effective medium permeability,

$$\bar{\epsilon}^{HU} = \epsilon_m \left(\frac{1 + \frac{1}{4}\sum_j f_j \alpha_j}{1 - \frac{1}{4}\sum_j f_j \alpha_j} \right)^2 . \quad (12)$$

This relation holds only for small filling factors.

C. Comparison of the theories

In the limit of small filling factor the MG-PvS, Bruggeman, and Hunderi theories all give the same effective medium permeability as is readily seen from Eqs. (8), (10), and (12), where the right members reduce to $\epsilon_m(1+\sum_j f_j \alpha_j)$. Such an identity is no longer found for larger f's. To demonstrate the differences we have computed $\bar{\epsilon}^{MG\text{-}PvS}$, $\bar{\epsilon}^{BR}$, and $\bar{\epsilon}^{HU}$ for identical spherical particles characterized by a Drude-type dielectric function $\epsilon = -10 + i$ in vacuum, i.e., with $\epsilon_m = 1$. Results for the real and imaginary parts ($\bar{\epsilon} = \bar{\epsilon}' + i\bar{\epsilon}''$) are given in Fig. 9 as a function of f. As expected, the three sets of curves are indistinguishable for sufficiently small filling factors. Specifically, if we require that $\bar{\epsilon}'$ and $\bar{\epsilon}''$ should differ by less than 10% for the three effective medium theories, we must have $f < 0.02$. It is also seen from Fig. 9 that the MG-PvS and Hunderi theories give rather similar results, whereas the Bruggeman theory consistently yields higher values of $\bar{\epsilon}$ as long as $f < 0.2$. For still larger f's ($0.2 < f \lesssim 0.8$), the MG-PvS and Hunderi theories lose their applicability entirely, while $\bar{\epsilon}^{BR}$ is found to exhibit a complex variation until it finally ends up, expectedly, as $\bar{\epsilon}^{BR} = -10 + i$ for $f = 1$.

The gas evaporated gold samples of the present investigation have f's of about $\frac{1}{300}$ (cf. Table I), and hence the three effective medium theories should all be equivalent. We would like to stress already at this stage, however, that all three theories are mean-field theories which neglect the nature of the local surrounding of the particles. As long as the average filling factor over a region comparable with the wavelength of the light is small, all theories give identical results because only the average f enters into the expressions. None of the theories can directly handle the situation where the particles are clustered, i.e., where there are local regions of high density, and none of the theories can therefore—as they stand—be expected to give a complete description of the experimental results. In Sec. VI C we will discuss a possible way of incorporating the effect of high local density.

It is seen from Fig. 9 that in the limit of small filling factor, $\bar{\epsilon}' \gg \bar{\epsilon}'' \propto f$ from which it follows that $\alpha \propto f$, where α is the absorption coefficient. From Eq. (1) this implies that $\alpha t \propto W/A$, i.e., the transmittance is given by the experimentally well-determined mass per unit area *but not* on the less precise values of f or t.

V. CALCULATIONS

In this section we present a series of calculations of optical properties using the three effective medium theories defined by Eqs. (8), (10), and (12). In Sec. A we specify the input parameters, which in essence amounts to choosing the best possible dielectric permeability for metal particles of size j. We also comment on the computational procedure. A preliminary comparison of theory and experiments is carried out in Sec. B where we find good agreement provided we: (i) use a fictitious plasma frequency for the particles which is smaller than in the bulk and (ii) take an effective optical thickness of the order of twice the measured one; the physical meaning of (i) and (ii) will be made clear in Sec. VI. In Sec. C we investigate the roles of particle diameter (mean value as well as distribution shape and width) and filling factor on the optical properties.

A. Input data and computational procedure

The frequency-dependent dielectric permeability for the individual gold particles is clearly of prime importance for the effective medium theories and hence in the calculation of optical properties. We chose to start from measured bulk data $\epsilon_{expt}(\omega)$—specifically we used highly accurate ellipsometric results by Winsemius[75]—

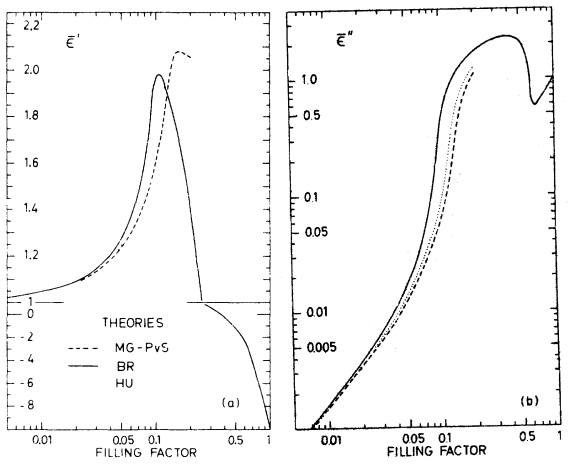

FIG. 9. Computed dielectric permeability for the MG-PvS, Bruggeman and Hunderi effective-medium theories as a function of filling factor. Part (a) shows the real part $\bar{\epsilon}'$ with a linear ordinate; note the different scales depending on whether $\bar{\epsilon}' > 1$ or $\bar{\epsilon}' < 1$. Part (b) shows the imaginary part $\bar{\epsilon}''$ with a logarithmic ordinate.

which were modified to account for size-dependent electron scattering in the Drude (free-electron) part of the dielectric function according to

$$\epsilon_j(\omega) = \epsilon_{\text{expt}}(\omega) - \epsilon_{\text{expt}}^{\text{Drude}}(\omega) + \epsilon_j^{\text{Drude}}(\omega). \quad (13)$$

It should be noted that this construction leaves the interband part of $\epsilon_{\text{expt}}(\omega)$ unchanged, which is justified as the *d*-band absorption in gold is quite insensitive to sample dimensions down to particle sizes of typically 1.5 nm. The two Drude terms in Eq. (13) are given by

$$\epsilon_{\text{expt}}^{\text{Drude}}(\omega) = 1 - \omega_{pb}^2/\omega(\omega + i/\tau_b) \quad (14)$$

and

$$\epsilon_j^{\text{Drude}}(\omega) = 1 - \omega_{pj}^2/\omega(\omega + i/\tau_j), \quad (15)$$

where ω_{pb} is the bulk plasma frequency, τ_b is the mean electron lifetime for bulk gold, ω_{pj} is the *apparent* plasma frequency for particles of size j, and τ_j is given by

$$\tau_j^{-1} = \tau_b^{-1} + 2v_{Fb}/x_j, \quad (16)$$

where v_{Fb} is the bulk Fermi velocity. This expression presumes[76] diffuse boundary scattering of the electrons in which case the mean free path is equal to the particle radius.[8,77,78]

From Winsemius[75] the bulk properties are

$$\hbar\omega_{pb} = 8.55 \text{ eV},$$

$$\hbar/\tau_b = 0.108 \text{ eV},$$

$$v_{Fb}/c = 4.7\times10^{-3}.$$

These have been used throughout our calculations and furthermore we always have

$$\epsilon_m = 1$$

in the effective medium treatments as the particles were surrounded by air (the slight modifications introduced by having a dielectric coating on the particles is discussed in Sec. VI A). Together with the parameter ω_{pj}, which for simplicity is taken to be a constant, and the sets of quantities $\{f_j; x_j\}$, which are specified by the experimental size distribution, these values allow a numerical evaluation of $\bar{\epsilon}^{\text{MG-PvS}}(\omega)$, $\bar{\epsilon}^{\text{BR}}(\omega)$, and $\bar{\epsilon}^{\text{HU}}(\omega)$.

Equations (8), (10), and (12) cannot be solved analytically for systems with a size distribution, but it is a straightforward matter to solve them by successive iterations. To do so we write them formally as

$$\bar{\epsilon}_n = F(\{f_j\}; \{\epsilon_j\}; \bar{\epsilon}_{n-1}), \quad (17)$$

where n denotes the iteration number, and put $\bar{\epsilon}_0 = \epsilon_m$. F is any of the functions on the right-hand sides of Eqs. (8), (10), or (12). The convergence is fast and to obtain

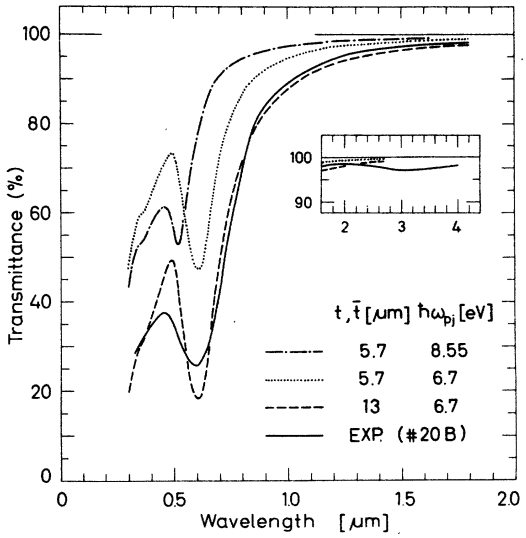

FIG. 10. Transmittance vs wavelength for sample No. 20 *B* in the ranges $0.3 < \lambda < 1.8$ μm and $1.8 < \lambda < 4$ μm (inset). Note that the horizontal scales are different. Solid curve represents measured data; this graph was shown previously in Fig. 6 and is reproduced here to allow comparison with the three other curves. These were calculated from the MG-PvS effective medium theory [Eq. (8)] using suitably modified bulk data for ϵ_j as described in Sec. V A. Size distribution was characterized by $\bar{x}$ and σ as given in Fig. 5 or in Table I. For the calculations we used $f = 0.005$ in addition to thickness (t respectively $\bar{t}$), and $\hbar\omega_{pj}$ as shown in the figure. By virtue of the small f no noticeable difference was observed for the Bruggeman and Hunderi theories.

$$|\bar{\epsilon}_n - \bar{\epsilon}_{n-1}| < 10^{-3}$$

only two iterations are necessary for $f = \frac{1}{200}$, whereas for $f = \frac{1}{10}$ n's up to seven are needed (depending on λ).

Once the dielectric functions for the effective media have been obtained, the corresponding frequency-dependent transmittances can be evaluated using the standard expressions for a thin film on a substrate.[79] The glass substrates were characterized by a refractive index of 1.4. We incorporated multiple reflections in the film but excluded interference effects in the substrate, i.e., we summed amplitudes in the thin film and intensities in the substrate.

B. Preliminary comparison of theory and experiments

Using the input data of Sec. V A in the effective medium theories of Sec. IV B we computed transmittance versus wavelength and compared with the experimental results described in Sec. III. Figure 10 shows a set of calculations with input parameters chosen to correspond to the measured

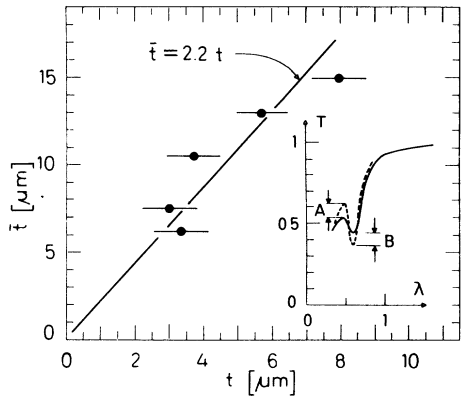

FIG. 11. Effective optical thickness $\bar{t}$ vs measured sample thickness t. Theoretical transmittance curves were fitted to the experimental data as in Fig. 10 until the vertical distances A and B were approximately equal; these two quantities are defined in the inset, where the dashed graph represents a computed wavelength-dependent transmittance, and the solid curve shows the measured behavior. Diagonal line represents Eq. (18).

size distribution of sample No. 20 B. Taking f to be 0.5% (cf. Table I) and using an unmodified plasma frequency for the particles, i.e., $\hbar\omega_{pj} = \hbar\omega_{pb} = 8.55$ eV, we arrived at the dash-dotted curve. Here we set $t = 5.7$ μm by which choice one gets agreement with the measured value of W/A [cf. Eq. (1)]. The most salient feature is the dip at $\lambda = 0.52$ μm. The minor shoulder at $\lambda = 0.35$ μm is a manifestation of a band-structure effect which is seen clearly also in bulk data (cf. the dotted curve in Fig. 1). Comparing with the measurements shown by the solid curve yields that the *qualitative* shapes of the theoretical and experimental graphs look similar, but that there exist two important *quantitative* discrepancies: the location of the transmittance minimum in the calculated curve occurs at too small wavelength, and the overall magnitude is approximately a factor twice too high! If the plasma frequency for the particles is adjusted, the transmittance dip is shifted, and for $\hbar\omega_{pj} = 6.7$ eV agreement is found for the locations of the minima as seen from the dotted curve in Fig. 10. If furthermore an effective optical thickness $\bar{t}$ is invoked, the magnitude of the transmittance can be fitted; taking $\bar{t} = 13$ μm brings the experimental data in fair correspondence with the computations as is evident from the dashed curve. The agreement is particularly good for $\lambda > 0.65$ μm, whereas the experimental curve looks considerably more smeared below this value, as might be blamed on a distribution of ω_{pj}'s. Clearly *this procedure to obtain agreement is very much ad hoc* and the meanings of $\omega_{pj} \neq \omega_{pb}$ and $\bar{t} \neq t$ need to be explained as will be done in Sec. VI where we consider dipole-dipole coupling between neighboring particles; however, the important point we want to make here is that *by choice of a fictitious plasma frequency for the particles which is lower than in the bulk and an effective thickness of the order of twice the measured one it is possible to bring the computed data into fair correspondence with the experiment.*

Fits similar to the one in Fig. 10 were carried out also for the samples Nos. 18 G, 19 A, 20 A, and 20 E. For the adjustable parameter ω_{pj} we consistently found

$$0.77 < \omega_{pj}/\omega_{pb} < 0.88$$

with no obvious dependence on sample thickness or any other characteristic quantity. The difference between ω_{pj} and ω_{pb} is much too large to be caused by a real shift of the plasma frequency. The effective thickness, as seen from Fig. 11, appeared to be related to the measured one by

$$\bar{t} = \eta t, \tag{18}$$

where the constant of proportionality is

$$\eta \approx 2.2.$$

C. Role of particle size and filling factor

Equation (16) shows that the electron scattering time and hence ϵ_j is influenced by the particle diameter. This effect modifies the optical properties as elaborated on in Fig. 12, where we have

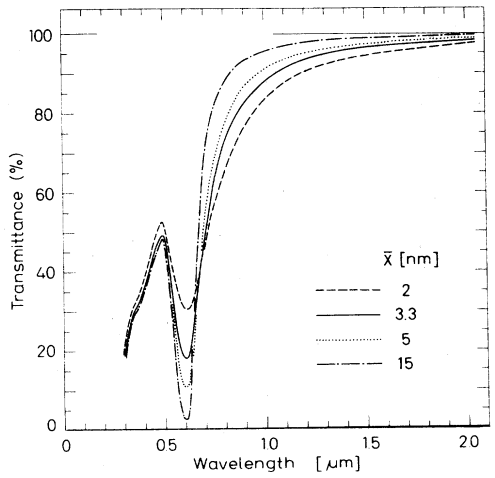

FIG. 12. Transmittance vs wavelength computed from the MG–PvS theory with $\bar{x}$ as shown in the figure, $\sigma = 1.40$, $\hbar\omega_{pj} = 6.7$ eV, $\bar{t} = 13$ μm, $f = 0.005$, and parameters for bulk gold. Solid line is identical with the dashed curve in Fig. 10.

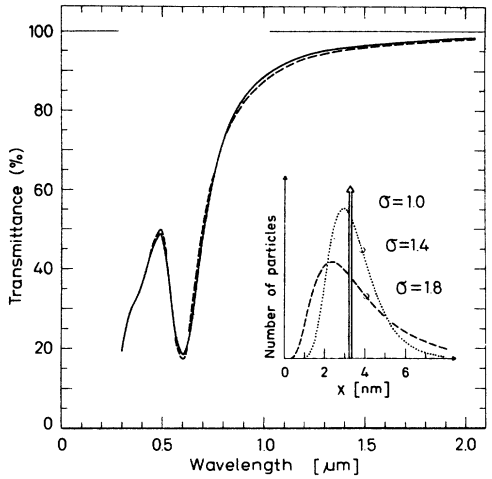

FIG. 13. Transmittance vs wavelength computed from the MG-PvS theory with $\bar{x}=3.3$ nm, σ as shown in the figure, and the rest of the parameters as in Fig. 12. Solid curve applies to $\sigma=1.0$ (or, more correctly, to $\ln\sigma=0.001$) and the dashed to $\sigma=1.8$. Corresponding size distributions are sketched in the inset, where we have also plotted a distribution for $\sigma=1.4$. Latter value is characteristic for our samples (cf. Fig. 5 and Table I) and has been included for comparison.

calculated wavelength-dependent transmittance as a function of median diameter $\bar{x}$ with log-normal size distributions having a constant geometric standard deviation $\sigma=1.40$. These computations were carried out with the same parameters as in Fig. 10, such that the curve for $\bar{x}=3.3$ nm is identical with the dashed curve in that figure. It is found in Fig. 12 that the shape of the transmittance minimum depends on $\bar{x}$ and gets progressively narrower and deeper as $\bar{x}$ is increased, whereas the location of λ_{min} is practically unchanged. The good agreement among the curves for $\lambda<0.5$ μm is a manifestation of the assumed size independence for the interband part of $\epsilon_{expt}(\omega)$. The highest median diameter we have considered, $\bar{x}=15$ nm, is on the verge for the effective medium theories to break down by the criterion in Sec. IV A.

Instead of varying $\bar{x}$, as in Fig. 12, we now keep $\bar{x}=3.3$ nm and look for the influence from an altered width of the size distribution. Figure 13 depicts transmittance versus wavelength for $\sigma=1.0$ (i.e., a δ function) and $\sigma=1.8$; the corresponding size distributions are sketched in the inset. Data for $\sigma=1.4$ are practically indistinguishable from those for $\sigma=1.0$. The particles having $x<\bar{x}$ will lead to a smoothing of the transmittance minimum, whereas those with $x>\bar{x}$ will yield a sharpening as was found in Fig. 12. Evidently these two counteracting effects result in the remarkable insensitiveness to the magnitude of the distribution width. Partly this is caused by the skewness of the log-normal distribution function, but the compensation is rather efficient also for symmetric distributions as was found from calculations where we used a Gaussian (mean value 3.3 nm and standard deviation 1.5 nm) or a triangular distribution (covering the interval $0<x<6.6$ nm). For any of these the computed transmittances deviated from the solid curve in Fig. 13 by less than 3% at all wavelengths.

It was pointed out in Sec. IV C that for filling factors of the order of 1% or less the precise value of f does not enter the problem of calculating transmittances as long as ft is proportional to the observed mass per unit area. We will now widen the scope of the discussion slightly and consider explicitly the role of a larger f. These computations are thus of minor interest in connection with our measurements but serve to illustrate some important features of the Bruggeman theory, which is the only one being strictly applicable for f's of the order of 0.1. The calculated results are presented in Fig. 14 where we have kept $f\bar{t}$ constant in order to get an appropriate normalization. For particles acting as independent scatterers the curves would then have been overlapping; such is practically the case for $f<0.02$ but for larger f's the data are seen to differ drastically. Figure 14 shows that by going to larger filling factors the magnitude of the transmittance is decreased and the mini-

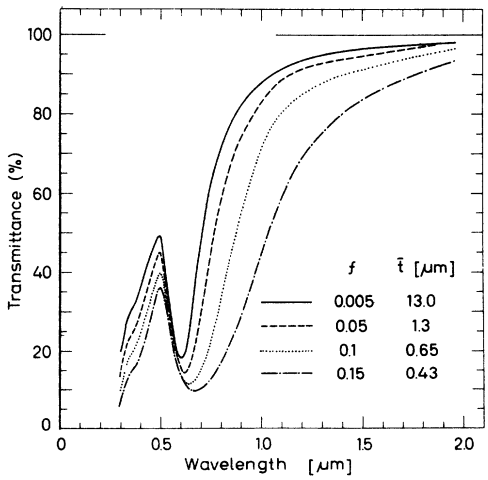

FIG. 14. Transmittance vs wavelength computed from the Bruggeman theory with $\bar{x}=3.3$ nm, $\sigma=1.40$, $\hbar\omega_{pj}=6.7$ eV, and parameters for bulk gold. Solid curve for $f=0.005$ and $\bar{t}=13$ μm is indistinguishable from the broken line in Fig. 10 which was obtained by use of the MG-PvS theory. Other three curves were computed with the shown values of f and t; these were chosen such that their product is invariant.

mum in the curves gets appreciably wider and shifts to somewhat larger λ_{min}'s.

VI. DISCUSSION

In Sec. V B we showed that the experimental transmittance data could be fitted to theory only by choosing empirical values for the plasma frequency ($\omega_{pj} < \omega_{pb}$) and the sample thickness ($\bar{t} > t$). This section will serve as an explanation for this approach. We consider the role of oxide coating (Sec. A) on the surfaces of the particles and the influence from nonspherical particle shapes (Sec. B). Both of these effects are capable of yielding a transmission minimum shifted to larger wavelengths, but detailed calculations disclose unambiguously that neither can account for our experimental results. We then regard *dipole-dipole interaction* between the particles in Sec. C. This effect may be important in our case *even* in the limit of very small filling factors, because most of the particles must indeed touch their neighbors in at least two points. Our discussion is based on a recent work by Clippe, Evrard, and Lucas[80] from which we extract a set of effective depolarization factors pertaining to geometrically well-defined aggregates of spheres. Presuming that a certain fraction of our deposits consists of close-packed clusters, another fraction consists of infinite chains, and the rest of the sample behaves as independent particles, we are able to obtain computed transmittance data which agree with experiments to within a few percent over the entire wavelength range. This proves hence that the theory of Secs. IV B and V A combined with an approximate treatment of dipole-dipole interaction is able to reproduce the measurements to within experimental uncertainties.

A. Oxide coating

Our ultrafine particles were prepared by evaporation in air which makes it plausible that at least a monolayer of oxide builds up on the surfaces of the individual grains, even if none could be observed by electron microscopy. The existence of some kind of dielectric coating was inferred previously from resistance measurements (cf. Sec. II A), and it was argued that this was due to an oxide rather than isolating WO_3 fragments, which are also present in the samples to some extent. To consider the role of oxide coverage we note that the α_j's [cf. Eq. (9)] have to be modified to incorporate the polarizability of a coated particle, whereas all other equations of the preceding sections can be taken over without changes. For a spherical particle covered with a concentric spherical shell with a dielectric constant ϵ^{ox} the polarizability is given by van de Hulst[61] and is proportional to

$$\alpha_j^{ox} = 3\,\frac{(\epsilon^{ox}-\bar{\epsilon})(\epsilon_j+2\epsilon^{ox})+q_j^3(2\epsilon^{ox}+\bar{\epsilon})(\epsilon_j-\epsilon^{ox})}{(\epsilon^{ox}+2\bar{\epsilon})(\epsilon_j+2\epsilon^{ox})+q_j^3(2\epsilon^{ox}-2\bar{\epsilon})(\epsilon_j-\epsilon^{ox})}, \tag{19}$$

with

$$q_j = 1-\frac{2t_{ox}}{x_j}, \tag{20}$$

where t_{ox} is the thickness of the oxide. In the limit of vanishing oxide thickness, i.e., for $q_j \to 1$, the expression in Eq. (9) is recovered (for $L_1 = L_2 = L_3 = \frac{1}{3}$) as it should.

With Eqs. (19) and (20) replacing Eq. (9) we have calculated wavelength-dependent transmittance from the formulas in Secs. IV and V using an unshifted plasma frequency, i.e., with $\hbar\omega_{pj} = \hbar\omega_{pb} = 8.55$ eV. The value of ϵ^{ox} must be fairly arbitrary as nothing appears to be known about the optical or electrical properties of any gold oxide.[43] In the computations we have set[81]

$$\epsilon^{ox} = 7,$$

which is of the same magnitude as for Cu_2O. Compared with many other oxides this is a high value and the choice should hence serve to maximize the influence from the dielectric. By having a nonzero t_{ox} the transmittance minimum is altered towards larger wavelengths, i.e., it acts to yield an *apparent* plasma frequency which is lower than in the bulk. This is illustrated in Fig. 15 where it is found that $t_{ox} = 0.9$ nm shifts λ_{min} to the same value as the experimentally observed one for sample No. 20 *B* (which we described, phenomenologically, as resulting from $\hbar\omega_{pj} = 6.7$ eV in Fig. 10). The relative amounts of oxide and metal are indicated by the cross-sectional view (inset) of a particle with a diameter equal to the median value.[82] The present mechanism for changing λ_{min} is incapable of directly explaining the magnitude of the transmittance, and the calculated curve (dotted) falls far above the experimental one (solid). It also goes well above the unshifted curve for $t_{ox} = 0$ (dash-dotted) which is obvious, as the amount of metal is decreased at the expense of an increased oxide thickness. Using, for a moment, an effective thickness $\bar{t} = 68$ μm we could shift the curve (dashed line) vertically such that an approximate correspondence with experiments was achieved. It should be noted that this value of $\bar{t}$ is more than an order of magnitude larger than the experimental one given by the measured mass per unit area, and it is also significantly larger than the one needed in our previous fit in Fig. 10. The approach is unsatisfactory not only because it requires $\bar{t} \gg t$,

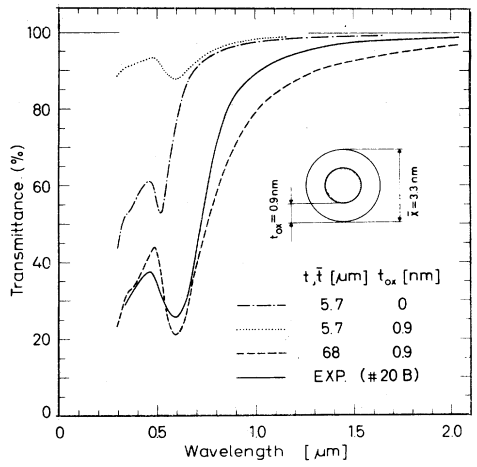

FIG. 15. Transmittance vs wavelength for oxide coated gold particles. Three theoretical curves were computed from the MG-PvS effective medium theory using $\epsilon^{ox}=7$, $\hbar\omega_{pj}=\hbar\omega_{pb}=8.55$ eV, $f=0.005$, $\bar{x}=3.3$ nm, $\sigma=1.40$, and with t, $\bar{t}$, and t_{ox} as shown in the figure. Inset depicts a cross section of an oxidized particle. By the above parameters the data for unoxidized grains (dash-dotted) are identical with the dash-dotted plot in Fig. 10. Curve for $t_{ox}=0.9$ nm and $\bar{t}=68$ μm (dashed) was fitted to the measured transmittance data for sample No. 20 *B* (solid) by the same criterion as in the inset of Fig. 11.

but it also leads to transmittance minima which are considerably wider than the experimentally observed ones. The effect is not unexpected since the decreased metal core diameters yield diminished τ_j's which lead to a smoothing of the curves as was elaborated on in Fig. 12. It should be stressed that even if we have neglected the imaginary part of ϵ^{ox}, this does not play any role in the shift of the absorption band as this is given by the real part of ϵ^{ox}. Furthermore, for any reasonable value of ϵ^{ox} the needed t_{ox}'s are much too large to be reconciled with the electron-microscopic evidence. We must then draw the conclusion that *an oxide coverage is responsible neither for the apparent shift of the plasma frequency nor for the occurrence of an effective thickness.*

B. Nonspherical particles

All previous computations of this paper have been devoted to spherical particles, although the effective medium theories in Sec. IV were written in a general form which remains valid[83] for ellipsoidal shapes [cf. Eq. (9)]. The restriction was motivated by the electron micrographs, where only well-rounded objects could be observed. The attainable resolution does not preclude some modest deviations from a spherical form, though.

In this section we will relax the requirement of spherical shapes and hence investigate the influence on the optical transmittance from depolarization factors L_1, L_2, and L_3 which differ from $\frac{1}{3}$. The normalization

$$\sum_{i=1}^{3} L_i = 1$$

is always valid. For all the effective medium theories the transmittance minimum occurs for $f \to 0$ when α_j has a maximum, i.e., when

$$\bar{\epsilon}(L_i - 1) = L_i \epsilon_j , \qquad (21)$$

as is easily verified from the equations of Sec. IV B, and it is obvious that λ_{min} will be affected by deviations from a spherical shape.

To see whether the occurrence of nonspherical particles is sufficient to account for the apparent shift of the plasma frequency and the effective sample thickness, we carried through a set of computations for prolate spheroids for which

$$L_1 < L_2 = L_3 ,$$

and for oblate spheroids defined by

$$L_1 = L_2 < L_3 .$$

Figure 16 depicts wavelength-dependent transmittance calculated for prolate spheroids using an unshifted plasma frequency, the experimental deposit thickness for sample No. 20 *B*, and de-

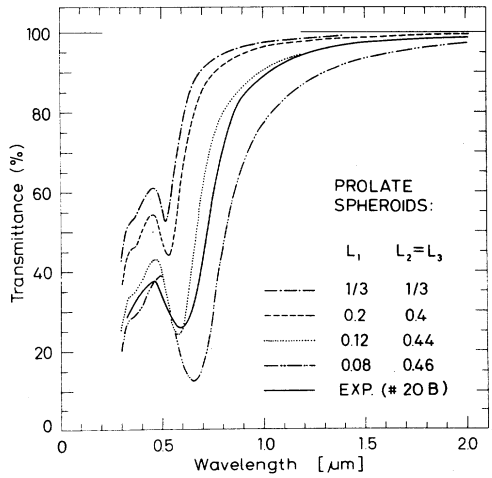

FIG. 16. Transmittance vs wavelength for nonspherical gold particles (prolate spheroids). Four theoretical curves were computed from the MG-PvS effective medium theory using $\hbar\omega_{pj}=\hbar\omega_{pb}=8.55$ ev, $t=5.7$ μm, $f=0.005$, $\bar{x}=3.3$ nm, $\sigma=1.40$, and L_1, L_2, and L_3 as given in the figure. Dash-dotted curve for $L_1=L_2=L_3=\frac{1}{3}$ (i.e. for spheres) is identical with the dash-dotted plot in Fig. 10. Solid curve represents measured data for sample No. 20 *B*.

polarization factors as shown in the figure. It is seen that when the ratio L_1/L_2 gets smaller (i.e., when the deviation from a spherical shape is enhanced) the location of λ_{min} shifts towards larger wavelengths and the overall magnitude of the transmittance is decreased. At $L_1 = 0.12$ and $L_2 = L_3 = 0.44$ (dotted curve) the correspondence with experimental data (solid curve) is rather good, and it may safely be surmised that an almost perfect fit could have been achieved by using a combination of two or more triplets of L_i's to describe a distribution of shapes. However, in order to see whether the agreement is meaningful we must now check if the above values of L_i, which are tantamount to a certain ratio between major (a) and minor (c) axes of the spheroid, can be reconciled with the electron microscopic data. For prolate spheroids (PS) of eccentricity

$$e_{PS} = [1 - (c/a)^2]^{1/2}, \tag{22}$$

the smallest depolarization factor is given by[84]

$$L_1 = \frac{1 - e_{PS}^2}{2e_{PS}^3}\left(\ln\frac{1+e_{PS}}{1-e_{PS}} - 2e_{PS}\right). \tag{23}$$

These equations were used to invert the λ_{min} vs L_1 relation, inherent in graphs of the kind shown in Fig. 16, to yield instead λ_{min} vs a/c data for PS's. As seen from Fig. 17 λ_{min} goes from the value 0.51 for spheres (cf. the dash-dotted curve in Fig. 16) up to 0.7 when $a/c = 5$. We also computed wavelength-dependent transmittance for oblate spheroids (OS) having various L_i's and

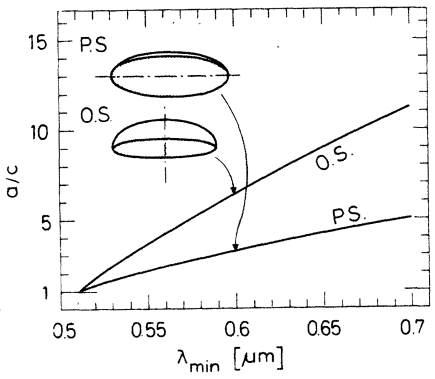

FIG. 17. Wavelength at the transmittance minimum (λ_{min}) vs the ratio between major and minor axes (a/c) for particles represented by prolate spheroids (PS) and oblate spheroids (OS). Graphs were obtained from a large set of curves similar to those in Fig. 16 and Eqs. (22)–(25). Inset depicts perspective sketches of half spheroids with a's and c's corresponding to $\lambda_{min} = 0.6$ μm (as indicated by the arrows). Two spheroids were drawn such that their volumes would be approximately equal; their axes of symmetry are denoted by dash-dotted lines.

extracted the corresponding λ_{min} vs L_3 variation by the relations[84]

$$L_3 = \frac{1+e_{OS}^2}{e_{OS}^3}(e_{OS} - \arctan e_{OS}), \tag{24}$$

with

$$e_{OS} = [(a/c)^2 - 1]^{1/2}. \tag{25}$$

The results are also included in Fig. 17. Experimentally we have $0.56 < \lambda_{min} < 0.6$ μm (cf. Sec. III), which from Fig. 17 corresponds to large ratios between major and minor axes both for prolate and oblate spheroids. The inset of Fig. 17 gives perspective sketches of half-spheroids pertaining to $\lambda_{min} = 0.6$ μm. Neither the very elongated shapes for PS's nor the flattened appearance for the OS's can be reconciled with the electron micrographs of Fig. 3(a), and in consequence the apparent shift of the plasma frequency and the effective sample thickness *cannot* be caused by nonspherical particles in spite of the good fit between theory and experiment which was evident from Fig. 16.

C. Role of dipole-dipole coupling and final comparison of theory and experiments

In the previous discussions it was tacitly presumed that the spatial distribution of particles was uniform throughout the sample. Considering the very small filling factors that were found experimentally this implies large intraparticle distances, in which case the local field is accurately approximated by the sum of the external field and the Lorentz field. From a direct inspection of typical electron micrographs [cf. Fig. 3(a)] it can be concluded that an assumption of large particle-particle distances must be a very crude one to the extent that it can be maintained at all, and it is evident that the individual particles stick together to form complex chains, clusters, etc. Consequently *dipole-dipole interaction* (or even higher multipole effects) *cannot be disregarded.*

Our semiquantitative description of the coupling is founded on a recent article by Clippe, Evrard, and Lucas,[80] who calculated the resonance frequency for several geometrical configurations of identical touching spheres such as doublets, linear triplets or quadruplets, spheres at the corners of an equilateral triangle or square or tetrahedron, an infinite single- or double strand chain, and a close-packed fcc lattice. Hence their calculation provides an explicit solution of Kirkwood's[85] theory for these particular spatial arrangements. We have attempted to account for dipole-dipole interaction by representing the computed[80] resonance frequencies by a set of *effective*

depolarization factors[86] L_i^*, which make the approach formally identical to the one for nonspherical particles; it is important to note, though, that the present depolarization factors are in a sense fictitious quantities which are not related to any ellipsoidal shapes. At least in the case of an infinite square lattice the effect of dipole-dipole interaction on the effective polarizability can be accounted for by introducing effective depolarization factors in the expression for the polarizability [i.e., our Eq. (9)] while all other formulas can be retained.[87] We feel that it is very plausible that the same applies in the present case. Clippe *et al.*[80] found, for example, that an infinite linear chain would inhabit three normal modes: one longitudinal at $\epsilon = -6.5\bar{\epsilon}$ and two transversal at $\epsilon = -1.3\bar{\epsilon}$. From Eq. (21) these results can be interpreted as resulting from $L_1^* = 0.133$ and $L_2^* = L_3^* = 0.435$. Similarly we have inverted the computed resonance frequencies for other pertinent configurations to yield the L_i^*'s compiled in Table II. It should be noted that a relation

$$\sum_{i=1}^{3} L_i^* \approx 1$$

is valid for all of these. For double spheres as well as for linear single-strand chains of infinite extension we find $L_1^* < L_2^* = L_3^*$, i.e., the aggregates behave like prolate spheroids as expected from the symmetry properties; more surprisingly the three-dimensional fcc lattice has $L_1^* = L_2^* < L_3^*$ such that it acts effectively as an oblate spheroid.

We used the same computational technique as in Sec. IV B to evaluate wavelength-dependent transmittance for samples assumed to consist entirely of double spheres, infinite linear chains with one strand, or a fcc lattice of spheres and applying the triplets of L_i^*'s in Table II, which were derived for identical spheres, also for our deposits which have a size distribution. From the results in Fig. 18 it is clear that, just as in Fig. 16, λ_{min} is shifted towards larger wavelengths and the overall transmittance is decreased as we go to aggregates characterized by smaller ratios L_1^*/L_2^* or L_2^*/L_3^*. The curve for double spheres (dotted) is seen to be very similar to the one for single independent spheres (dashed). When many more particles are hooked on to form a long straight chain the computed data stand in fair, though not perfect, agreement with experimental results for sample No. 20 *B* (solid curve). The same is equally true for double-strand chains (for clarity these results are not shown). For a fcc lattice, finally, the theoretical curve drops well below the measured one.

To get a final comparison of theory and experiments we considered the sample to be a mixture of aggregates with several geometrically well-determined configurations. Specifically we chose single spheres, linear infinite chains, and clusters having a fcc lattice. The existence of such structures in the deposits was documented by the electron micrographs [cf. Fig. 3(a)]. Double spheres and double-strand chains were not included in the discussion owing to the small differences with single spheres and single-strand chains, respectively, for the transmittance data. In the final fit we hence required that the filling factor would be

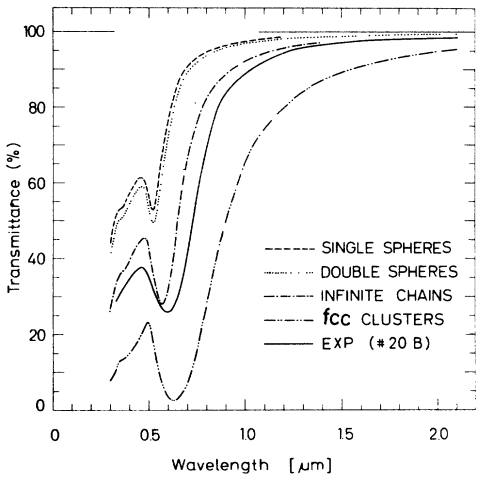

FIG. 18. Transmittance vs wavelength for ultrafine gold particles with dipole-dipole interaction. Four theoretical curves were computed from the MG-PvS effective medium theory with the same parameters as in Fig. 16 and with L_1^*, L_2^*, and L_3^* as contained in Table II. Dashed curve for single independent spheres is identical with the dash-dotted plot in Fig. 10. Curve for linear infinite chains with one strand is very similar to the dotted curve in Fig. 16 by virtue of their practically equal depolarization factors. Solid graph represents experimental results for sample No. 20 *B*.

TABLE II. Equivalent depolarization factors for different geometrical configurations of identical spheres as extracted from Ref. 80.

Geometrical configuration	⟨Equivalent depolarization factor⟩ L_1^*	L_2^*	L_3^*
Single sphere	$\frac{1}{3}$	$\frac{1}{3}$	$\frac{1}{3}$
Double sphere	0.250	0.375	0.375
Single strand chain	0.133	0.435	0.435
Double strand chain	0.139	0.342	0.518
fcc lattice	0.0865	0.0865	0.827

ξf for single spheres;

ζf for infinite chains;

$(1-\xi-\zeta)f$ for fcc clusters;

where $\xi, \zeta \geq 0$ and $\xi + \zeta \leq 1$. This procedure introduces two adjustable parameters ξ and ζ just as we had two parameters ω_{pj} = constant and $\bar{t}$ in the preliminary comparison of theory and experiments in Sec. V B. The main advantages with the present approach are twofold: (i) a much better fit can be achieved as will be proved shortly and (ii) the parameters ξ and ζ have a precise physical meaning. It should be pointed out, though, that ξ and ζ do not necessarily represent exactly the "true" fractions of single spheres or infinite chains in the samples, because we have not attempted to incorporate any relative absorption strengths for the different aggregates. The two parameters should then be interpreted as, loosely speaking, the product of an "oscillator strength" and a "true" fractional filling factor. In practice this does not play any role as the "true" fractions of the different geometrical configurations are not any experimentally accessible quantities. Furthermore it has been shown by Vlieger[87] and by Yamaguchi[16] for the two-dimensional case that the right oscillator strength is obtained by using only an effective depolarization factor. We believe the same to be true for our experimental situation, and hence the correction caused by varying absorption strength for the separate geometrical configurations should be a small effect.

Figure 19 depicts calculated wavelength-dependent transmittances with parameters chosen to correspond to those for samples Nos. 18 *G* and 20 *B*. With the shown percentages of single spheres, infinite linear chains, and close-packed fcc clusters it is clear that we can bring the computed results into *very good agreement* with the measured data over the *whole* wavelength interval. The fits are not completely unique as a small increase of the single sphere fraction at the expense of a corresponding decrease of the fcc portion does not lead to any significant modifications, as may be understood from the graphs in Fig. 18. However, Fig. 19 proves unambiguously that roughly half of the sample can be described as consisting of long linear chains, whereas for the rest of the deposit we can assign approximately equal amounts of single spheres and fcc clusters. This result is not contradicted by the electron micrographs. The strongest deviations between theory and experiments are found consistently in the interval $0.45 < \lambda < 0.50$ μm, where the computed data overshoot the experimental by up to 6% as can be seen from Fig. 19. Also in the

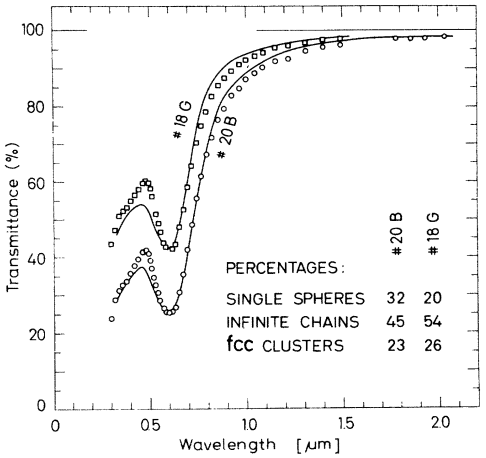

FIG. 19. Measured and computed transmittance vs wavelength curves for ultrafine gold particles with dipole-dipole interaction. Solid plots were shown previously in Fig. 6. Closely resembling theoretical data (squares and circles) were obtained from the MG-PvS effective medium theory with $\hbar\omega_{pj} = \hbar\omega_{pb} = 8.55$ eV, $f = 0.005$, $t(18G) = 2.5$ μm, $t(20B) = 5.7$ μm [which gives agreement with the measured W/A's by Eq. (1)], $\bar{x}$ and σ for the two samples as given in Table I, and L_i^*'s for single spheres, infinite single strand chains, and fcc clusters as contained in Table II. Shown percentages for these geometrical configurations were used. Slight scatter of the theoretical data from a smooth variation (particularly manifest around $\lambda = 1$ μm) and the gap at $1.5 \gtrsim \lambda \gtrsim 1.8$ μm reflect uncertainties in the ellipsometric results for $\epsilon_{expt}(\omega)$ as reported by Winsemius (Ref. 75).

range $0.85 < \lambda < 1.1$ μm there appears to be a slight though systematic discrepancy and the experimental transmittancies are larger than the calculated ones. For other wavelengths the correspondence can be made virtually perfect by a proper selection of ξ and ζ. The deviations are probably caused by the strong simplification in regarding dipole-dipole coupling for only three different geometrical configurations, whereas in reality there must be a wide spectrum including chains, rings, and clusters of all shapes and sizes with, in general, multipole-multipole interaction.

We would like to stress, that we feel that our approach to treat dipole-dipole interactions certainly involves more than mere curve fitting. The *only* parameters entering the calculations are ξ and ζ, whereas we used experimental values for t, f, size distribution, and bulk dielectric function (in Sec. V B, t and ω_{pj} were taken to be adjustable parameters). With only two parameters we fit well a large number of characteristic features of the spectra; for the absorption band centered at about 600 nm we get the right position, width, and absolute transmittance value; we also

reproduce accurately features of both the infrared and ultraviolet transmittance.

VII. SUMMARY AND CONCLUDING REMARKS

In this paper we have addressed ourselves to the old problem of the "anomalous absorption," which has been seen frequently in systems comprised of noble-metal aggregates (the probably incomplete listing in Sec. I contained over 50 articles published during the last two decades). In order to obtain a sufficiently simple experimental system to permit a detailed *quantitative* comparison of theory and experiments we prepared ultrafine gold particles using gas evaporation following, in essence, a technique due to Harris,[29] whereby complicating effects from a medium surrounding the granules can be avoided and highly accurate samplings of the deposits can be achieved by straightforward electron microscopy. For colloidal particles in a glass matrix, to pick one of the alternative preparation techniques, the sample must be pulverized mechanically and the glass dissolved before microscopy can commence, which is bound to introduce unrepresentative samplings caused by coagulation. The main disadvantage with gas evaporation is that the particles must be touching at *any* filling factor, whereas a more even spatial distribution can probably be obtained by most other techniques. We feel, however, that this drawback is outweighed by the more precise sample analysis, which in our case allowed us to determine not only an average diameter of the single-crystalline spherical particles but we also documented that the size distributions were accurately log-normal. Using a combination of optical microscopy and weighings we determined the deposit thickness and filling factor, the latter being of the order of 0.3%. Optical transmittance was measured by standard techniques. Provided the deposits were sufficiently thin we obtained very reproducible readings with a marked transmittance minimum at a wavelength of about 0.6 μm; for thicker layers the particles coagulated into large aggregates presumably caused by the combined effects of heating from the vapor source and a substantial melting point depression in minute gold particles.

As a foundation for the theoretical description of the wavelength-dependent transmittances we formulated three prescriptions to get an average dielectric permeability, which defines an "effective medium," from the permeabilities of the metal particles and their surroundings (i.e., air), respectively. Specifically we adopted the effective medium theories due to Maxwell–Garnett[57] in conjunction with Polder and van Santen,[67] Bruggeman,[58] and Hunderi.[59] A general criterion for their validity was put forward. The basic self-consistent equations [Eqs. (8)–(10) and (12)] were written in a novel manner which points up their similarities and differences and which is particularly convenient for computations when size distributions and/or ellipsoidal particles need to be considered. In the limit of vanishing filling factors the effective medium theories become identical and they all represent an exact solution of Maxwell's equations. The most crucial part of the theory is the choice of a dielectric permeability for the metal particles. We used Winsemius's[75] ellipsometrically determined data for bulk gold, which we believe to be more accurate than previous results,[88] and modified the free-electron part to incorporate the effect of a size-dependent mean-free path, presuming diffuse boundary scattering of the electrons. Hence we neglected any change in the interband part of the dielectric function as well as quantum size effects. The computed results exhibited a transmittance minimum which resembled the experimentally observed one. We found that the minimum got narrower and deeper as the median diameters were increased, which is a simple manifestation of the enhanced mean free paths; more remarkable was the extreme insensitiveness to the width of the log-normal distributions.

In order to produce a good fit between theory and experiments it was necessary to invoke: (i) a *fictitious plasma frequency* which was lower than the bulk value, and (ii) an *effective sample thickness* of the order of twice the measured one.

To understand the background of these seemingly bizarre and unphysical effects we first considered the influence from the dielectric coating on the particles. By explicit calculations we demonstrated that a shift of the transmittance minimum towards larger wavelengths (i.e., an apparently lowered plasma frequency) could occur, whereas no enhanced thicknesses could be obtained, simply because the nonabsorbing dielectric is produced at the expense of a decrease for the absorbing metal cores. The effects (i) and (ii) could be accounted for formally by presuming nonspherical particle shapes, but correspondence with experiments could be reached only by postulating very oblong or flattened particles for which no evidence was gained from the electron micrographs, and hence this explanation must be discarded too. We finally elucidated the role of *dipole-dipole interactions*, which were represented by introducing triplets of effective depolarization factors pertaining to each of a set of well-defined geometrical configurations of spheres. The dis-

cussion was based on a theoretical work by Clippe *et al.*[80] Our approach, which we believe has not been adopted before, was to consider the deposit as consisting of close-packed clusters, infinite linear chains, and single particles, whose relative amounts were taken to be adjustable parameters. From this procedure we were able to get *computed data which agreed with the experiments to within a few percent over the entire wavelength range* by using only physically plausible input parameters. For completeness it should be mentioned that the decrease of the electron concentration at the surfaces of a particle, which takes place over typically a Thomas–Fermi screening length, may also alter the transmittance minimum as was pointed out recently[89]; the effect is probably too small to be of any significance for our samples, though.

Evidence for an apparent decrease of the plasma frequency in gold aggregates has been found previously in several experiments[25,90,91] probing the optical properties. Sometimes this has been interpreted as caused by an "optical" mass for the electrons being much larger than the free-electron value, but the origin of such an enhancement has not been made clear. These results were all obtained for discontinuous films or granular deposits, whereas no increased "optical" mass was found in well-crystallized films.[92] In our opinion this indicates that the shift of the plasma frequency is an *apparent* rather than a real effect caused by either dipole-dipole coupling, nonspherical shapes, or oxide coatings on the particles, or several of these effects in combination. The same might be the reason also behind the shifted transmittance minima found recently in ultrafine Ag and Na particles by Smithard *et al.*[7,93]

It is of prime importance that our extremely good agreement between theory and experiments could be obtained *without* incorporation of any quantum size effects but only properly modified bulk data. At first sight this might seem surprising as the particles are sufficiently small for the normally quasicontinuous conduction band to break up into distinct levels with non-negligible separations.[94,95] Hence the surfaces should not act as simple scatterers but rather to determine the eigenstates for the electrons. Presuming a Poisson distribution of completely nondegenerate eigenvalues Kawabata and Kubo[96] calculated the dissipation caused by dipole transitions by use of linear response theory. Their approach was improved on by Gor'kov and Êliashberg,[97] who pointed out that the random level separation can be refuted on very general grounds, and instead the two-level distribution function should obey either of three separate statistical ensembles, which lead to different dielectric permeabilities (depending on atomic spin-orbit coupling and external magnetic field). Recently two alternative and much simpler quantum-mechanical derivations of the dielectric function were provided by Cini and Ascarelli[98] and by Genzel *et al.*[9] To reproduce our experimental data we needed neither of these sophisticated theories but, as stressed above, we relied successfully on the classical theory in combination with measured bulk results.

One possible reason for the absence of quantum size effects in our data might be that the individual energy levels overlap completely at room temperature. It would therefore be interesting to extend the transmittance measurements to lower temperatures. Experiments by Kreibig[8] and by Scheunemann and Jäger[13] on the optical absorption in ultrafine silver particles at liquid-helium and at room temperature did not exhibit any drastically

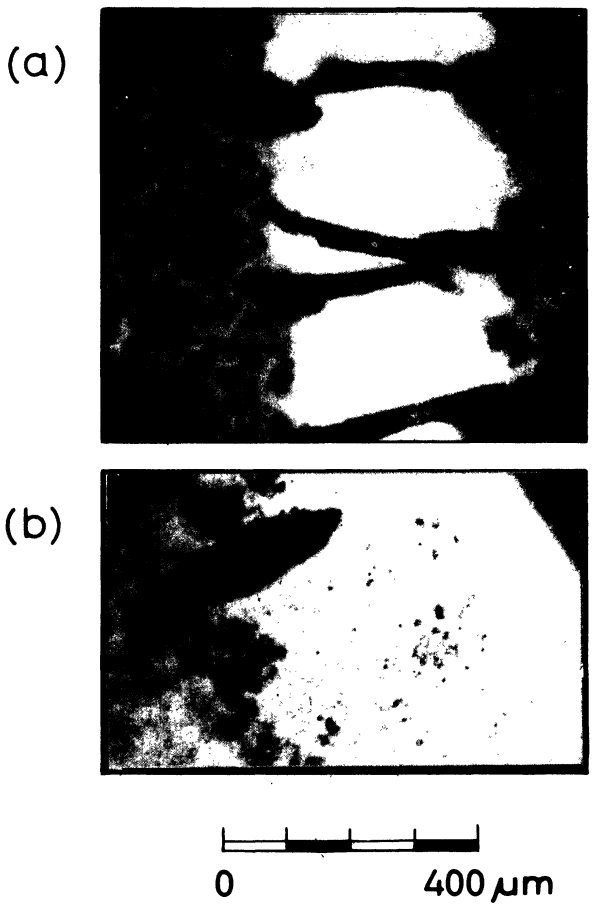

FIG. 20. Structure of gold deposits, produced by evaporation in air, studied at scratches made in sample No. 20 *B* [part (a)] and sample No. 20 *A* [part (b)]. Dark regions at the corners are caused by the small aperture in the optical microscope.

differing results, which could have been taken as evidence for an onset of quantum size effects, but our improved theoretical and experimental analyses should make a renewed attempt worthwhile. An even more crucial probe of the elusive quantum effects is to study the absorption of far-infrared radiation at frequencies comparable with the mean energy spacing. A recent reappreciation[99] of previous measurements[40] at low temperatures disclosed severe discrepancies between experiments and the Gor'kov–Éliashberg theory,[97] and the classical theory for the electrons is probably superior also in the far-infrared regime, as will be discussed in a forthcoming article.

ACKNOWLEDGMENTS

We are very grateful to Professor A. A. Lucas for giving us a preprint of Ref. 80 and to Dr. H. P. Lengkeek for sending us a computer printout of ellipsometric data for bulk gold. The transmittance determination for a gold film in Fig. 1 was kindly provided by Dr. P. O. Nilsson.

APPENDIX: PARTIAL COLLAPSE OF THE STRUCTURE

Some interesting effects were observed when a scratch, made with a needle in the porous deposit consisting of Au particles, was studied by optical microscopy. Figure 20(a) shows results for sample No. 20 *B* which was previously reported on in Fig. 2. The microscope was focused 3.5 μm above the substrate plane and hence the structure should look similar to the one in Fig. 2(b). This is true for the two regions close to the vertical sides of the picture, which signify the untransformed part. The central region shows the scratch; evidently the original deposit has collapsed into a series of horizontal structures which on close inspection appear to be hollow. The filling factor for these "tubes" (assuming circular cross sections) was estimated to be three to four times larger than for the original layer. This observation agrees with the previous report[40] of f's being of the order of percent for particle films which had been scraped off their backing.

Figure 20(b) shows a similar scratch made in sample No. 20 *A*. The microscope was focused in the substrate plane. The lightest irregular areas to the right are caused by the needle hitting the glass surface. This region is surrounded by a rather wide gray zone indicating a thin and even coating. To the left remnants of the original structure are visible in addition to a collapsed "tube" which is of the same nature as those described in Fig. 20(a). Clearly the particles closest to the substrate adhere rather strongly whereas the others, which form a series of clusters, can get wiped off more easily. These conclusions substantiate the conceptual model for the deposits which was depicted by the line drawings of Fig. 2.

---

*Supported by the Swedish National Science Research Council.

†Present address: Dept. of Physical Metallurgy, Norwegian Institute of Technology, Trondheim, Norway.

[1]C. v. Fragstein and H. Römer, Z. Physik 151, 54 (1958); H. Römer and C. v. Fragstein, *ibid.* 163, 27 (1961); C. v. Fragstein and F. J. Schoenes, *ibid.* 198, 477 (1967).

[2]U. Kreibig and P. Zacharias, Z. Phys. 231, 128 (1970).

[3]R. H. Doremus, J. Chem. Phys. 40, 2389 (1964).

[4]R. Yokota and K. Shimizu, J. Phys. Soc. Jpn. 12, 833 (1957).

[5]R. H. Doremus, J. Chem. Phys. 42, 414 (1965).

[6]U. Kreibig and C. v. Fragstein, Z. Phys. 224, 307 (1969).

[7]M. A. Smithard and R. Dupree, Phys. Status Solidi A 11, 695 (1972); M. A. Smithard, Solid State Commun. 13, 153 (1973); J.-D. Ganière, R. Rechsteiner, and M. A. Smithard *ibid.* 16, 113 (1975).

[8]U. Kreibig, J. Phys. F 4, 999 (1974).

[9]L. Genzel, T. P. Martin, and U. Kreibig, Z. Phys. B 21, 339 (1975).

[10]W. Kleeman, Z. Phys. 215, 113 (1968).

[11]S. C. Jain, N. D. Arora, and K. L. Chaudri, J. Appl. Phys. 45, 2368 (1974); S. C. Jain and N. D. Arora, Solid State Commun. 15, 433 (1974).

[12]D. C. Skillman and C. R. Berry, J. Chem. Phys. 48, 3297 (1968).

[13]W. Scheunemann and H. Jäger, Z. Phys. 265, 441 (1973).

[14]G. C. Papavassiliou, J. Phys. F 6, L103 (1976).

[15]There is a large amount of old work. For references see, for example, H. Mayer, *Physik Dünner Schichten* (Wissenschaftlische Verlagsgesellschaft, Stuttgart, 1950), Vol. 1, p. 226 ff.; O. S. Heavens, *Optical Properties of Thin Solid Films* (Dover, New York, 1965), p. 161 ff.

[16]T. Yamaguchi, J. Phys. Soc. Jpn. 15, 1577 (1960); 17, 184, 1172 (1962); 18, 226 (1963); Oyo Buturi 44, 64 (1975); S. Yoshida, T. Yamaguchi, and A. Kinbara, J. Opt. Soc. Am. 61, 62, 463 (1971); 62, 634, 1415 (1972); T. Yamaguchi, S. Yoshida, and A. Kinbara, Jpn. J. Appl. Phys. 8, 559 (1969); Thin Solid Films 13, 261 (1972); 18, 63 (1973); 21, 173 (1974); J. Opt. Soc. Am. 64, 1563 (1974).

[17]W. Fleichsig, Z. Phys. 162, 570 (1961); 170, 176 (1962); 176, 380 (1963); 191, 423 (1966); 200, 304 (1967).

[18]G. Rasigni and P. Rouard, J. Opt. Soc. Am. 53, 604 (1963); P. Payan and G. Rasigni, J. Phys. Radium 25, 92 (1964); P. Rouard and G. Rasigni, Opt. Acta 14, 27 (1967).

[19]R. H. Doremus, J. Appl. Phys. 37, 2775 (1966).

[20]N. Emeric and A. Emeric, Thin Solid Films 1, 13 (1967).

[21]A. Carlan, Ann. Phys. (Paris) 4, 5 (1969).

[22]J. P. Marton, J. Appl. Phys. 40, 5383 (1969); R. W. Tokarsky and J. P. Marton, J. Vac. Sci. Technol. 12, 643 (1975).
[23]J. P. Gasparini and R. Fraisse, Thin Solid Films 30, 111 (1975).
[24]S. L. McCarthy, J. Vac. Sci. Technol. 13, 135 (1976).
[25]V. V. Truong and G. D. Scott, J. Opt. Soc. Am. 66, 124 (1976).
[26]W. Hampe, Z. Phys. 152, 470, 476 (1958).
[27]R. W. Cohen, G. D. Cody, M. D. Coutts, and B. Abeles, Phys. Rev. B 8, 3689 (1973).
[28]E. B. Priestley, B. Abeles, and R. W. Cohen, Phys. Rev. B 12, 2121 (1975).
[29]L. Harris, R. T. McGinnies, and B. M. Siegel, J. Opt. Soc. Am. 38, 582 (1948); L. Harris, D. Jeffries, and B. M. Siegel, J. Appl. Phys. 19, 791 (1948).
[30]L. Harris and J. K. Beasley, J. Opt. Soc. Am. 42, 134 (1952).
[31]L. Harris, *The Optical Properties of Metal Blacks and Carbon Blacks* (The Eppley Foundation for Research, Monograph Series No. 1, Newport, R.I., 1967).
[32]V. N. Sintsov, Zh. Priklad. Spektrosk. 4, 503 (1966) [J. Appl. Spectrosc. 4, 362 (1966)].
[33]D. R. McKenzie, J. Opt. Soc. Am. 66, 249 (1976).
[34]C. G. Granqvist and O. Hunderi, Solid State Commun. 19, 939 (1976); J. Phys. (Paris) (to be published).
[35]J. R. Sambles, Proc. R. Soc. Lond. 324, 339 (1971); Ph. Buffat and J.-P. Borel, Phys. Rev. A 13, 2287 (1976). Typically the melting point is depressed to 70% of its bulk value when the diameter is 3 nm.
[36]K. Kimoto, Y. Kamiya, M. Nonoyama, and R. Uyeda, Jpn. J. Appl. Phys. 2, 702 (1963); K. Kimoto and I. Nishida, *ibid.* 6, 1047 (1967).
[37]S. Yatsuya, S. Kasukabe, and R. Uyeda, Jpn. J. Appl. Phys. 12, 1675 (1973); S. Kasukabe, S. Yatsuya, and R. Uyeda, *ibid.* 13, 1714 (1974).
[38]C. G. Granqvist and R. A. Buhrman, J. Appl. Phys. 47, 2200 (1976); R. A. Buhrman and C. G. Granqvist, *ibid.* 47, 2220 (1976). The first paper contains an extensive listing of references to previous works.
[39]I. N. Stranski and L. Krastanov, Sitzungsber. Akad. Wiss. Wien, Math.—Naturwiss. Kl. IIb 146, 797 (1938). A more accessible account is given by E. Bauer [Z. Kristallogr. 110, 372 (1958)].
[40]D. B. Tanner, A. J. Sievers, and R. A. Buhrman, Phys. Rev. B 11, 1330 (1975).
[41]P. G. Wilkinson, J. Appl. Phys. 22, 226 (1951).
[42]E. Ando, Jpn. J. Appl. Phys. 11, 986 (1972).
[43]Gold oxides with the compositions Au_2O, AuO, and Au_2O_3 are mentioned in G. V. Samsonov [*The Oxide Handbook* (IFI/Plenum, New York, 1973)].
[44]R. S. Roth and J. L. Waring, J. Res. Nat. Bur. Stands. A 70, 281 (1966). See, alternatively, ASTM cards 20—1323 and 20—1324.
[45]R. Uyeda, J. Crystal Growth 24/25, 69 (1974).
[46]C. G. Granqvist and R. A. Buhrman, Solid State Commun. 18, 123 (1976).
[47]C. G. Granqvist and R. A. Buhrman, Appl. Phys. Lett. 27, 693 (1975).
[48]T. Andersson and C. G. Granqvist, J. Appl. Phys. (to be published).
[49]C. G. Granqvist and R. A. Buhrman, J. Catalysis 42, 477 (1976).
[50]E. K. Plyler and J. J. Ball, J. Opt. Soc. Am. 38, 988 (1948); L. Harris, D. Jeffries, and B. M. Siegel, J. Chem. Phys. 18, 261 (1950); L. Harris and A. L. Loeb, J. Opt. Soc. Am. 43, 1114 (1953); L. Harris and K. F. Cuff, *ibid.* 46, 160 (1956); L. Harris, *ibid.* 51, 80 (1961).
[51]W. R. Blevin and W. J. Brown, Metrologia 2, 139 (1966).
[52]A theory for the optical properties of the gold blacks was developed by G. Zaeschmar and A. Nedoluha [J. Opt. Soc. Am. 62, 348 (1972)].
[53]L. C. Roess and E. N. Dacus, Rev. Sci. Instrum. 16, 164 (1945).
[54]C. B. Aiken, W. H. Carter, Jr., and F. S. Phillips, Rev. Sci. Instrum. 17, 377 (1946).
[55]H. E. Stubbs and R. G. Phillips, Rev. Sci. Instrum. 31, 115 (1960).
[56]A summary of many different theories can be found in L. K. H. van Beek [Progr. Dielectr. 7, 69 (1967)], or in W. R. Tinga, W. A. G. Voss and D. F. Blossey [J. Appl. Phys. 44, 3897 (1973)].
[57]J. C. Maxwell-Garnett, Phil. Trans. R. Soc. Lond. 203, 385 (1904); 205, 237 (1906). The basic relation [our Eq. (7)] was first derived by J. W. Rayleigh, Philos. Mag. 34, 481 (1892). A recent discussion has been given by L. Genzel and T. P. Martin, Surf. Sci. 34, 33 (1973).
[58]D. A. G. Bruggeman, Ann. Phys. (Leipz.) 24, 636 (1935).
[59]O. Hunderi, Phys. Rev. B 7, 3419 (1973).
[60]G. Mie, Ann. Phys. (Leipz.) 25, 377 (1908).
[61]H. C. van de Hulst, *Light Scattering by Small Particles* (Wiley, New York, 1957).
[62]E. David, Z. Phys. 114, 389 (1939).
[63]H. Schopper, Z. Phys. 130, 565 (1951).
[64]J. P. Marton and J. R. Lemon, Phys. Rev. B 4, 271 (1971).
[65]L. Onsager, J. Am. Chem. Soc. 58, 1486 (1936).
[66]C. J. F. Böttcher, Rec. Trav. Chem. 64, 47 (1945); *Theory of Electric Polarisation* (Elsevier, Amsterdam, 1952), Sec. 64.
[67]D. Polder and J. H. van Santen, Physica (Utrecht) 12, 257 (1946).
[68]To obtain self-consistency we let $\bar{\epsilon}$ replace the original [cf. Eq. (13) in Ref. 67] ϵ_m in the nominator.
[69]V. I. Odelevskii, J. Tech. Phys. 21, 678 (1951).
[70]R. Landauer, J. Appl. Phys. 23, 779 (1952).
[71]S. Kirkpatrick, Phys. Rev. Lett. 27, 1722 (1971).
[72]R. J. Elliott, J. A. Krumhansl, and P. L. Leath, Rev. Mod. Phys. 46, 465 (1974).
[73]D. Stroud, Phys. Rev. B 12, 3368 (1975); D. Stroud and F. P. Pan, *ibid.* B 13, 1434 (1976).
[74]M. H. Cohen and J. Jortner, Phys. Rev. Lett. 30, 696 (1973); J. Phys. (Paris) 35, C4-345 (1974); J. Jortner and M. H. Cohen, Phys. Rev. B 13, 1548 (1976).
[75]P. Winsemius, Ph.D. thesis (Rijksuniversiteit te Leiden, the Netherlands, 1973) (unpublished).
[76]Considering the electrons to be scattered according to a Lambert cosine law leads to a prefactor $\frac{3}{2}$ in the last term of Eq. (16) (cf. Ref. 8). We believe this possibility to be less probable than diffuse boundary scattering.
[77]J. Euler, Z. Phys. 137, 318 (1954).
[78]W. T. Doyle, Phys. Rev. 111, 1067 (1958).
[79]See, for example, O. S. Heavens, *Optical Properties of Thin Solid Films* (Dover, New York, 1965).
[80]P. Clippe, R. Evrard and A. A. Lucas, Phys. Rev. B 14, 1715 (1976).

[81]If the dielectric coating is not a gold oxide but WO_3, the use of a real ϵ^{ox} is inappropriate as tungsten trioxide is strongly absorbing at $\lambda \lesssim 0.5\,\mu$m (cf. Ref. 33). Existence of such an absorption for Au particles is difficult to check owing to the strong interband absorption. However, we have very recently investigated the optical properties of silver particles prepared by the technique described in this paper. The interband contribution for Ag sets in only at $\lambda \lesssim 0.3\,\mu$m. No absorption attributable to WO_3 was seen in these experiments which makes us convinced that it is negligible also for the present work. These considerations motivate our choice of ϵ^{ox}.

[82]It is assumed that the particle diameter, as seen in the electron microscope, includes the oxide layer. Alternatively one could have assumed that x denotes only the metal core outside which the oxide is grown; however, we find it very unlikely that the oxide would not have been detected in bright field micrographs if it were as thick as approximately 1 nm, and hence the latter hypothesis was rejected.

[83]A minor problem is caused by the proper definition of τ_j for nonspherical particles. For simplicity we have used Eq. (16) without changes although a better definition would have been $\tau_j^{-1} = \sum_{i=1}^{3} \tau_{ij}^{-1}/3$ with $\tau_{ij}^{-1} = \tau_b^{-1} + 2v_{fb}/x_{ij}$, where x_{ij} denotes the lengths of the three perpendicular axes of an ellipsoidal particle. The diameters x_j in the size distribution should be interpreted as $x_j = (\prod_{i=1}^{3} x_{ij})^{1/3}$.

[84]L. D. Landau and E. M. Lifshitz, *Electrodynamics of Continuous Media* (Pergamon, New York, 1960), Sec. 4.

[85]J. G. Kirkwood, J. Chem. Phys. 4, 592 (1936); see also Sec. 41 in Böttcher's book (Ref. 66).

[86]The concept of the effective depolarization factor has been used previously by Yamaguchi *et al.* (Ref. 16) and by A. Meessen [J. Phys. (Paris) 33, 371 (1972)]. It was recently applied to the optical properties of discontinuous gold films by Truong and Scott (Ref. 25).

[87]J. Vlieger, Physica (Utrecht) 64, 63 (1973); see also D. Bedaux and J. Vlieger, *ibid.* 73, 287 (1974).

[88]See, in particular, B. R. Cooper, H. Ehrenreich, and H. R. Philipp, Phys. Rev. 138, A494 (1965).

[89]R. Ruppin, J. Opt. Soc. Am. 66, 449 (1976).

[90]V. G. Padalka and I. N. Shklyarevskii, Opt. Spektrosk. 11, 527 (1961) [Opt. Spectrosc. 11, 285 (1961)].

[91]B. Dold and R. Mecke, Optik 22, 435 (1965).

[92]M.-L. Thèye, Phys. Rev. B 2, 3060 (1970) and references therein.

[93]M. A. Smithard and M. Q. Tran, Helv. Phys. Acta 46, 869 (1974).

[94]H. Fröhlich, Physica (Utrecht) 4, 406 (1937).

[95]R. Kubo, J. Phys. Soc. Jpn. 17, 975 (1962).

[96]A. Kawabata and R. Kubo, J. Phys. Soc. Jpn. 21, 1765 (1966).

[97]L. P. Gor'kov and G. M. Éliashberg, Zh. Eksp. Teor. Fiz. 48, 1407 (1965) [Sov. Phys.–JETP 21, 940 (1965)].

[98]M. Cini and P. Ascarelli, J. Phys. F 4, 1998 (1974).

[99]C. G. Granqvist, R. A. Buhrman, J. Wyns, and A. J. Sievers, Phys. Rev. Lett. 37, 625 (1976); J. Phys. (Paris) (to be published).

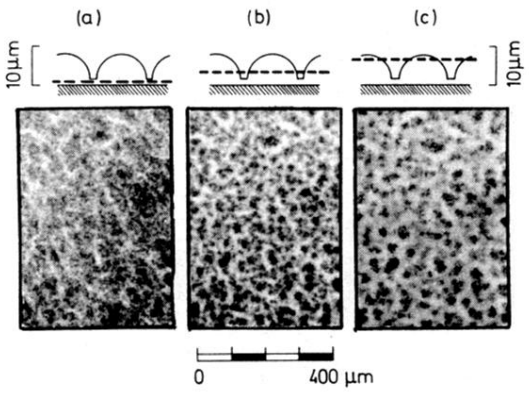

FIG. 2. Microscope images of the same region of a gold deposit prepared by evaporation in air (sample No. 20 *B*). Schematic upper pictures show a cross-sectional view of particle layers on glass substrates. Dashed lines indicate focal planes for the microscope.

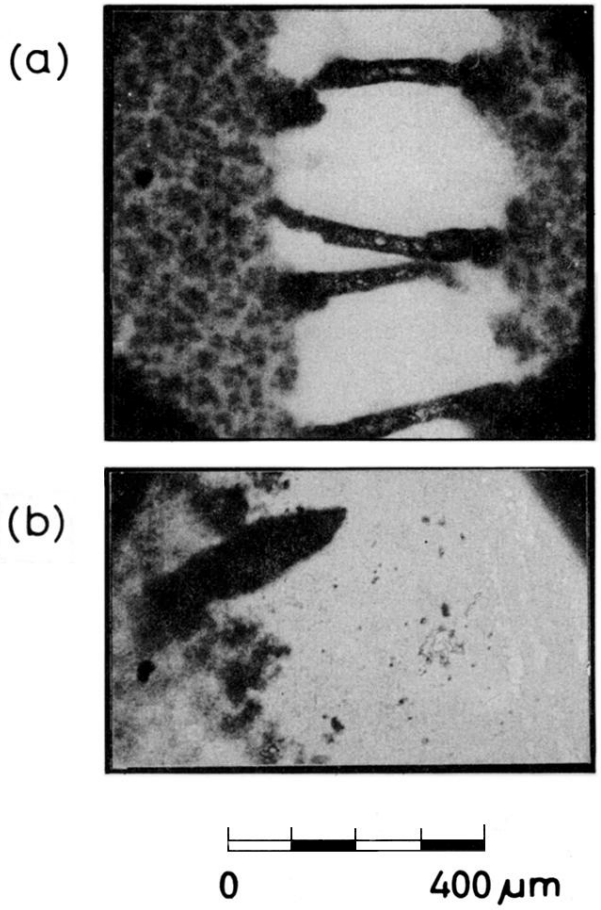

FIG. 20. Structure of gold deposits, produced by evaporation in air, studied at scratches made in sample No. 20 *B* [part (a)] and sample No. 20 *A* [part (b)]. Dark regions at the corners are caused by the small aperture in the optical microscope.

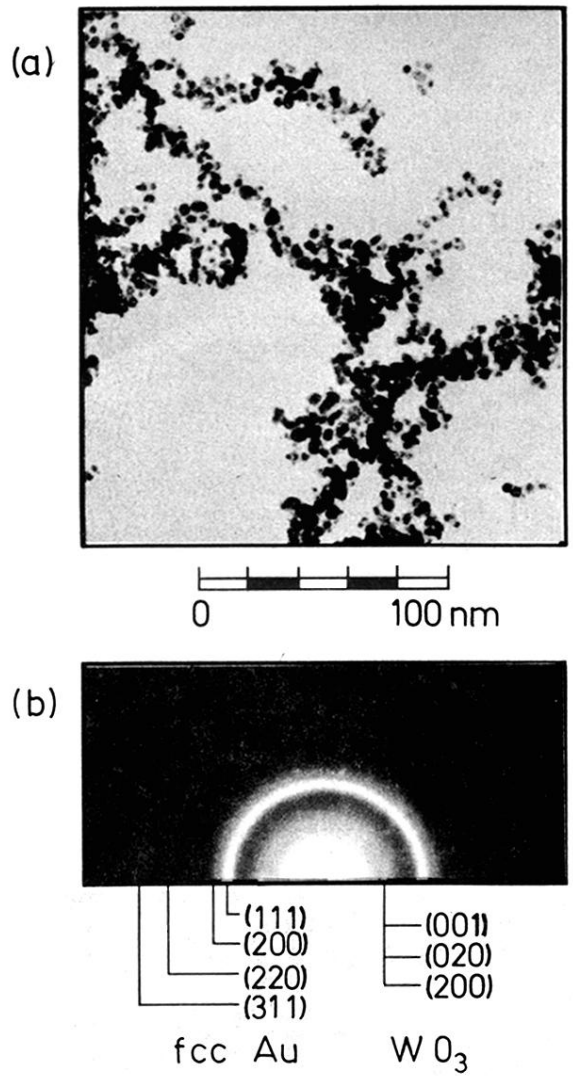

FIG. 3. Part (a) depicts ultrafine gold particles prepared by evaporation in air (sample No. 20 *B*). Note the clusters and chains! Grainy background is caused by structure in the supporting carbon layer. Part (b) shows electron diffraction from the same sample. Calculated positions for the four innermost reflections of fcc Au are indicated; these agree with the measured radii. Correspondence was obtained also for the line intensities. Weak line closest to the center is due to three overlapping reflections from triclinic and/or orthorhombic WO_3 (cf. Ref. 44).

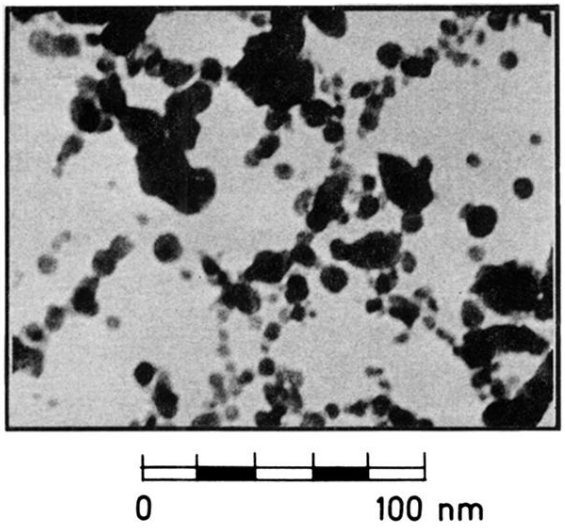

FIG. 4. Coagulated gold particles prepared by evaporation in air (sample No. 18 *H*). Largest particles exhibit a tendency towards hexagonal images which is probably indicative of their being three-dimensional icosahedrons (cf. Ref. 45).